universität wien

MASTERARBEIT / MASTER'S THESIS

Titel der Masterarbeit / Title of the Master's Thesis

"Mineralogical Characterization of Sulfidic Mine Waste of the Abandoned Copper Deposit Gornja Lipa, Bor District, Serbia"

verfasst von / submitted by

Tamina Josefa Buttinger-Kreuzhuber, Bsc

angestrebter akademischer / in partial fulfilment of the requirements for the degree of

Master of Science (MSc)

Wien, 2016 / Vienna, 2016

Studienkennzahl lt. Studienblatt / degree programme code as it appears on the student record sheet:	A 066 815
Studienrichtung lt. Studienblatt / degree programme as it appears on the student record sheet:	Masterstudium Erdwissenschaften UG2002
Betreut von / Supervisor:	Ao. Univ-Prof. Dr. Christian L. Lengauer
Mitbetreut von / Co-Supervisor:	Dr. Tamara Đorđević

Acknowledgements

First and foremost I want to thank Tamara Đorđević for providing the possibility to work on this very interesting topic and the continuous support during the working process. Further I want to thank Uwe Kolitsch for the constructive help with the work for this master thesis, especially the measurements on the scanning electron microscope and the interpretation of the data. Additionally, I want to thank Christian Lengauer for the support with my master thesis, and the help with the powder X-ray diffraction measurements.

I am also very grateful for the technical and scientific help provided by Dan Topa, Gerald Giester, Aleksandar Pačevski, Andreas Artač, and Andreas Wagner.

Finally I want to thank my parents Katharina and Johannes, my sister Mira and my partner Helmut for their strong support during this challenging time in my life.

Declaration

I declare that this thesis was written by myself and it does not contain material, which has been submitted or accepted for an award of any other degree or diploma in any university or institution. All cited literature is listed in the bibliography without exception. To the best of my knowledge and belief this thesis contains no material previously published by any other person except where acknowledgments and references have been made.

Vienna, 2016

_____

Tamina Buttinger-Kreuzhuber

Abstract

The aim of this master thesis is a thorough characterization of the mineralogical composition of solid waste material of the abandoned Gornja Lipa deposit in East Serbia using different analytical techniques (SEM-EDS, powder and single-crystal XRD, reflected-light microscopy, X-ray fluorescence spectroscopy, Raman spectroscopy).

The Gornja Lipa deposit is a high-sulfidation epithermal porphyry copper deposit and belongs to the Bor metallogenic zone. The deposit, where active mining operations were ongoing until the mid-1960s, is a massive to disseminated mineralization in hydrothermally altered volcanic rocks. The ore body, which was pyritized, silicified, kaolinized and alunitized, consists mainly of pyrite, enargite and luzonite, and subordinate to trace arsenopyrite, bornite, chalcopyrite, stibnite, colusite, galena, sphalerite, and tennantite. The accompanying minerals comprise quartz, muscovite, kaolinite, diaspore, and pyrophyllite, with accessory rutile, barite, fluorapatite, titanite and aluminium phosphate-sulphate (APS) minerals (crandallite, goyazite, svanbergite, woodhouseite). Several of these species are newly reported for the deposit.

Judging from the mineralogy of the deposit, it was expected to find the secondary Fe-arsenate-hydrate scorodite, as it represents a typical weathering product of Fe- and As-bearing deposits, but no scorodite could be found. This could be explained by the small amount of samples analyzed. A continuing study with a larger amount of samples would probably detect the presence of scorodite. The As-minerals enargite, tennantite arseonpyrite and colusite were identified; as As-bearing minerals pyrite with up to ~3,2 at.% As, antimonite with up to ~2.5 at.% As and limonite with up to ~0.24 at.% As were observed

The occurrence of APS minerals along with abundant kaolinite, diaspore, and pyrophyllite indicates conditions of argillic to advanced argillic alteration which can be linked to high-sulfidation epithermal copper mineralizations.

Zusammenfassung

Das Ziel dieser Masterarbeit war eine gründliche Charakterisierung der mineralogischen Zusammensetzung von Abraumproben der stillgelegten Lagerstätte Gornja Lipa im Osten Serbiens mittels verschiedener Analysetechniken (REM-EDS, Pulver- und Einkristall-Röntgendiffraktometrie, Erzmikroskopie, Röntgenfluoreszenz-Spektroskopie, Raman-Spektroskopie).

Die Lagerstätte Gornja Lipa ist eine „high-sulfidation“ epithermale, porphyrische Kupferlagerstätte und gehört zur metallogenischen Zone von Bor. Die Lagerstätte wurde bis zur Mitte der 1960er Jahre abgebaut und stellt eine massive bis disseminierte Mineralisation in hydrothermal alterierten, vulkanischen Gesteinen dar. Der Erzkörper ist pyritisiert, silifiziert, kaolinitisiert und alunitisiert und besteht hauptsächlich aus Pyrit, Enargit und Luzonit. Untergeordnet sind Arsenopyrit, Bornit, Chalkopyrit, Antimonit, Colusit, Galenit, Sphalerit und Tennantit vorhanden. Die Begleitminerale der Gangart sind Quarz, Muskovit, Kaolinit, Diaspor und Pyrophyllit. Akzessorisch sind Rutil, Baryt, Fluorapatit, Titanit und Aluminium-Phosphat-Sulfat (APS)-Minerale (Crandallit, Goyazit, Svanbergit, Woodhouseit) vorhanden. Mehrere dieser Spezies sind Neubestimmungen für die Lagerstätte.

Aufgrund der Mineralogie der Lagerstätte wäre das Auftreten von Skorodit zu erwarten, da dieser ein typisches Verwitterungsprodukt von Fe- und As-führenden Lagerstätten darstellt. Es wurde jedoch kein Skorodit gefunden. Grund dafür könnte die geringe Anzahl an analysierten Proben sein. Eine weiterführende Untersuchung mit größerer Probenanzahl würde wahrscheinlich das Auftreten von Skorodit belegen. Es wurden die As-Minerale Enargit, Tennantit, Arsenopyrit und Colusit identifiziert; als As-führende Minerale wurden Pyrit mit bis zu 3,2 at.% As, Antimonit mit bis zu 2,5 at.% As und Limonit mit bis zu 0,24 at.% As identifiziert.

Das Vorkommen von APS-Mineralen zusammen mit reichlich vorkommendem Kaolinit, Diaspor und Pyrophyllit weisen auf argillitische bis fortgeschrittene argillitische Alterations-Bedingungen hin, diese können mit den „high-sulfidation“ epithermalen Kupfermineralisationen in Verbindung gebracht werden.

Table of contents

1. Introduction

1.1. Formation of high-sulfidation epithermal deposits

Epithermal deposits form at relatively shallow depths from the Earth's surface to a depth of 1 to 2 km in a temperature range of 150°C to 300°C in the course of hydrothermal alteration (White and Hedenquist, 1995). They are commonly classified into three subgroups: high-, intermediate- and low-sulfidation epithermal deposits, which differ in their associated alteration halo and sulfide mineralogy (White and Hedenquist, 1995; Hedenquist et al., 2000; Einaudi et al., 2003).

Low-sulfidation epithermal deposits are characterized by a reduced fluid with low salinity and near neutral pH. Typically pyrite, arsenopyrite, and sphalerite are found, less common tetrahedrite-tennantite. Indicating the near neutral pH the gangue minerals are mainly banded veins of quartz, adularia, and especially calcite. They occur preferably in continental and island-arc rifts with bimodal volcanism (White and Hedenquist. 1995; Sillitoe and Hedenquist, 2003).

Intermediate-sulfidation epithermal deposits are set in between the sulfidation state of low- and high-sulfidation epithermal deposits. They are found in calc-alkaline, andesitic-dacitic arcs, but often also in felsic rocks. The mineral associations consist of chalcopyrite, tetrahedrite-tennantite, and sphalerite (Sillitoe and Hedenquist, 2003).

High-sulfidation epithermal deposits are typically found in calc-alkaline andesitic-dacitic island arc terranes and continental margins (Sillitoe and Hedenquist, 2003; Hedenquist et al., 2000), together with permeable lithologies or near volcanic vents to allow fast upward transport of magmatic fluids (Fig. 1.; Hedenquist et al., 2002). They are often bound to porphyry copper deposits and may occur in lithocaps of advanced argillic alteration above the porphyry copper system (Sillitoe, 2010). Some examples have no apparent association with subvolcanic intrusions (e.g. *Nalesbitan*, *Nansatsu*; Arribas, 1995). Arribas (1995) points out that most deposits are of tertiary age, while only few examples of mesozoic (e.g. *Pueblo Viejo, Zijinshan*), paleozoic (e.g., *Temora*) or precambrian (e.g. *Enåsen*) age exist.

The mineralization of high-sulfidation deposits shows a great variety in the structure of the ore bodies including veins, hydrothermal breccias, stockworks, disseminations and replacements (Arribas, 1995).

The magmatic fluids altering the wall rocks are oxidizing (SO_2, SO_4^{2-}, H_2SO_4), with low pH (1-3) and moderate salinity. A characteristic zoning of the host rocks is introduced by the cooling fluid, leaving in the end only silica behind, most often with a vuggy texture. With the cooling of the fluid, metals (Au, Ag, Cu, As) are precipitated within the silica-rich host rock. The commonly accepted theory of high-sulfidation epithermal ore-deposit evolution is an early leaching and alteration stage grading into a later ore-forming stage (Arribas, 1995). The typical mineral association consists of sulfide-rich assemblages, namely pyrite-enargite, pyrite-luzonite, pyrite-famatinite and pyrite-covellite (Neukirchen and Ries, 2014). Covellite is rather rare and appears very late in the mineralizing sequence, normally emplaced in vugs (Einaudi et al., 2003).

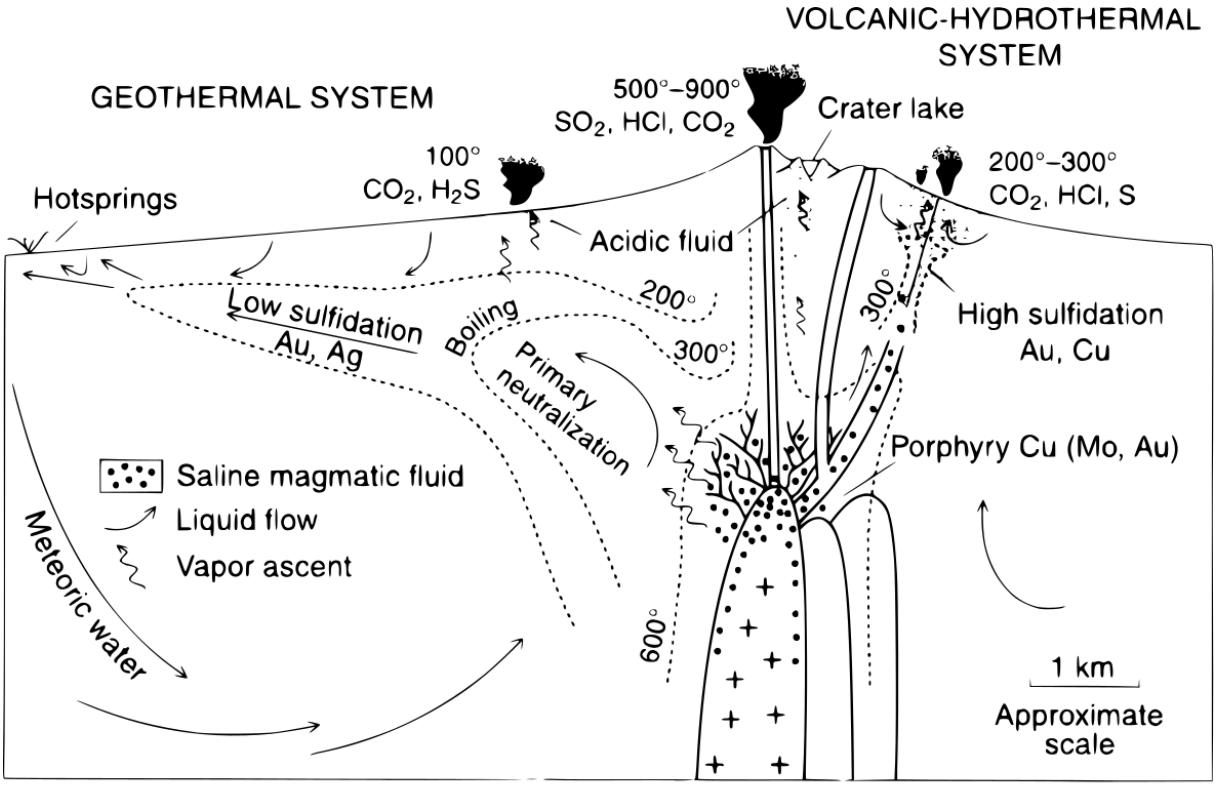

Fig. 1. Formation of high- and low-sulfidation epithermal deposits in relationship to a porphyric intrusion in a volcanic-hydrothermal and geothermal system (Hedenquist et al., 2000).

The accompanying minerals are closely associated with the advanced argillic alteration zone. Those minerals are quartz, alunite, pyrophyllite and/or dickite, indicative of low pH values in the fluid. Barite is usually introduced very late (Einaudi et al., 2003). The economic important ore is mainly found in the vuggy quartz zone (Sillitoe and Hedenquist, 2003).

Some famous examples of these epithermal deposits are El Indio (Chile), Pueblo Viejo (Dominican Republic), Summitville (Colorado, USA), Goldfield (Nevada, USA), Lepanto (Philippines) and Lahóca (Hungary) (White and Hedenquist, 1995)

1.2. Alteration zones in high-sulfidation epithermal deposits

The lateral outward alteration zoning of the host rock induced by acidic fluids is characteristic in high-sulfidation epithermal deposits. As outlined by Hedenquist et al. (2000), fluids generally originate from three different sources; they may come from hypogene magmatic condensates, steam-heated oxidation or supergene oxidation (Table 1). The advanced argillic alteration of barren lithocaps and high-sulfidation epithermal deposits is formed by hypogene magmatic condensates, while blankets of advanced argillic alteration over high- and low-sulfidation deposits may be formed by steam-heated oxidation or supergene oxidation. Indicative for hypogene origin is the occurrence of true residual silica, whereas steam-heated alteration should not display residual silica, although there may be a porous texture due to the steam-heated alteration. Additionally, alunite formed by steam-heated alteration exhibits a characteristic pseudocubic or rhombohedral crystal habit.

Table 1. Defining characteristics of acid alteration (Table modified from Hedenquist et al., 2000).

	Hypogene chloride-sulphate	Steam-heated sulphate	Supergene
Genetic terminology (Rye et al., 1992)	Magmatic-hydrothermal	Steam-heated	Supergene
Origin	Condensation of high-T magmatic vapor with HCl + SO_2 ascending	Atmospheric oxidation of H_2S in vadose zone above water table	Atmospheric oxidation of fine-grained sulfide within surficial weathering zone
Temperature range	300° - 350° to 100°C, ascending hypogene fluid	100° - 120°, up to 150°C, descending fluid	20°-10°C, overprinting descending fluid
Assemblages	Quartz, alunite, kaolinite, dickite, diaspore, pyrophyllite, zunyite	Kaolinite, alunite, opal, cristobalite, native sulfur	Kaolinite, halloysite, jarosite
Relationship to ore	Potentially ore-bearing, typically forms envelope to ore	Barren, above ore or overprint	Unrelated to sulfide ore, related to oxide ore

In a volcanic hydrothermal environment the acidic fluid is responsible for leaching the wall rock, the remainder is a residual silicic core with vuggy texture. This core is encompassed by an advanced argillic alteration halo (Fig. 2.), which is characteristic for high-sulfidation epithermal deposits. These specific alteration zone sequence is useful for the exploration geologist to identify the ore-bearing zones, as they can be used as “spatial markers” (Arribas, 1995). The vuggy quartz zone is enclosed by a zone of advanced argillic alteration composed of quartz-alunite and clay minerals (kaolinite, nacrite and dickite) as well as pyrophyllite and diaspore. This advanced argillic alteration zone is also found in patches of the vuggy quartz zone, referable to local zones of lower permeability, which forestalled a complete leaching of the silicic zone. Outwards follows the argillic alteration zone consisting of quartz, kaolinite, illite, and additionally smectite and sericite. The outermost zone, the prophyllitic alteration zone, carries chlorite, smectite, and sometimes carbonates (Arribas, 1995; Hedenquist et al., 2000). Characteristic are in outward direction mineral assemblages of decreasing pH values.

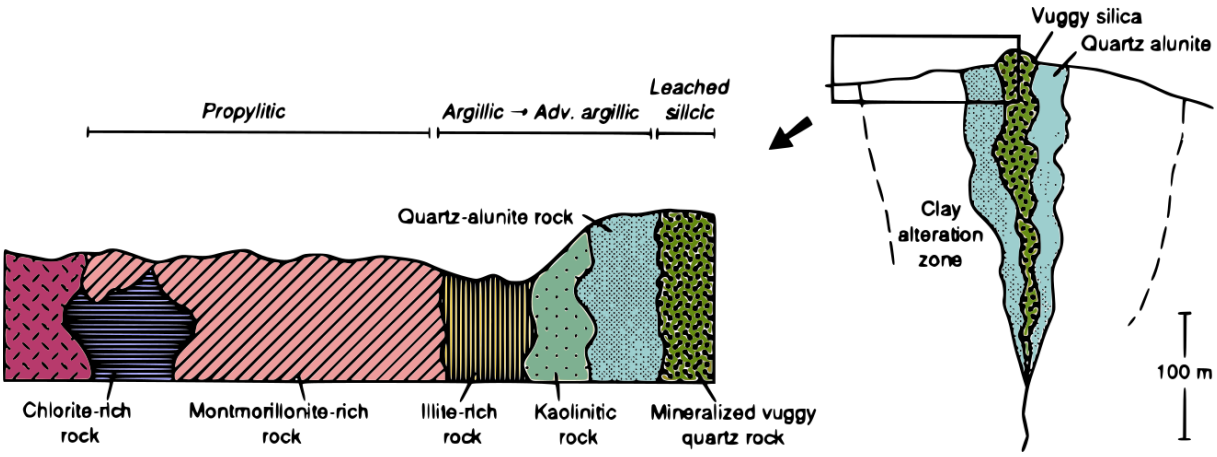

Fig. 2. Schematic drawing of alteration zones visible at the high-sulfidation Au-Cu-deposit, Summitville, Colorado. Typical outward alteration zoning with the ore mineralization located in the vuggy quartz zone (modified after Arribas, 1995, Steven and Ratté, 1960; Stoffregen, 1987).

Downwards, the alteration zones are similar to the lateral direction with a shallow silicic zone giving way to the advanced argillic, argillic, argillic/sericitic zones, and eventually into a sericitic or phyllic zone. These changes occur over a span of few hundred up to 1000 m (Arribas, 1995).

1.3. Banatitic Magmatic and Metallogenetic Belt (BMMB) - geological setting

The Banatitic Magmatic and Metallogenetic Belt (BMMB) (Berza et al., 1998) or Apuseni-Banat-Timok-Srednogorie belt (Strashimirov and Popov, 2000) is a 1500 km long and 30 to 70 km wide ore-bearing igneous belt in south-eastern Europe. It extends in north-south orientation from Romania to Serbia and in east-western orientation to Bulgaria (Fig. 3). The formation of the belt is dated to the "[…] subduction of the Vardar Ocean during the Late Cretaceous, as part of the closure of the Neothetys that had separated Europe and Africa during the Mesozoic" (Ciobanu et al., 2002). The complex tectonic history of the subduction is still subject to debate (e.g. Linzer et al., 1998; Zweigel et al., 1998, Hippolyte et al., 1999; Neugebauer et al., 2001; Săndulescu and Visarion, 2000). Intrusive and extrusive calc-alkaline magmatism took place over a time period from ~90 to ~60 Ma (Ciobanu et al., 2002). The L-shaped belt hosts numerous magmatic-hydrothermal Cu, Au, Mo, Zn, Pb and Fe deposits. These deposits are not placed continuous within the belt but rather clustered irregularly (Fig. 3). The most important deposits in the BMMB region are porphyry Cu and associated high-sulfidation epithermal deposits, massive sulfide, skarn and vein deposits (Heinrich and Neubauer, 2002; Berza et al., 1998).

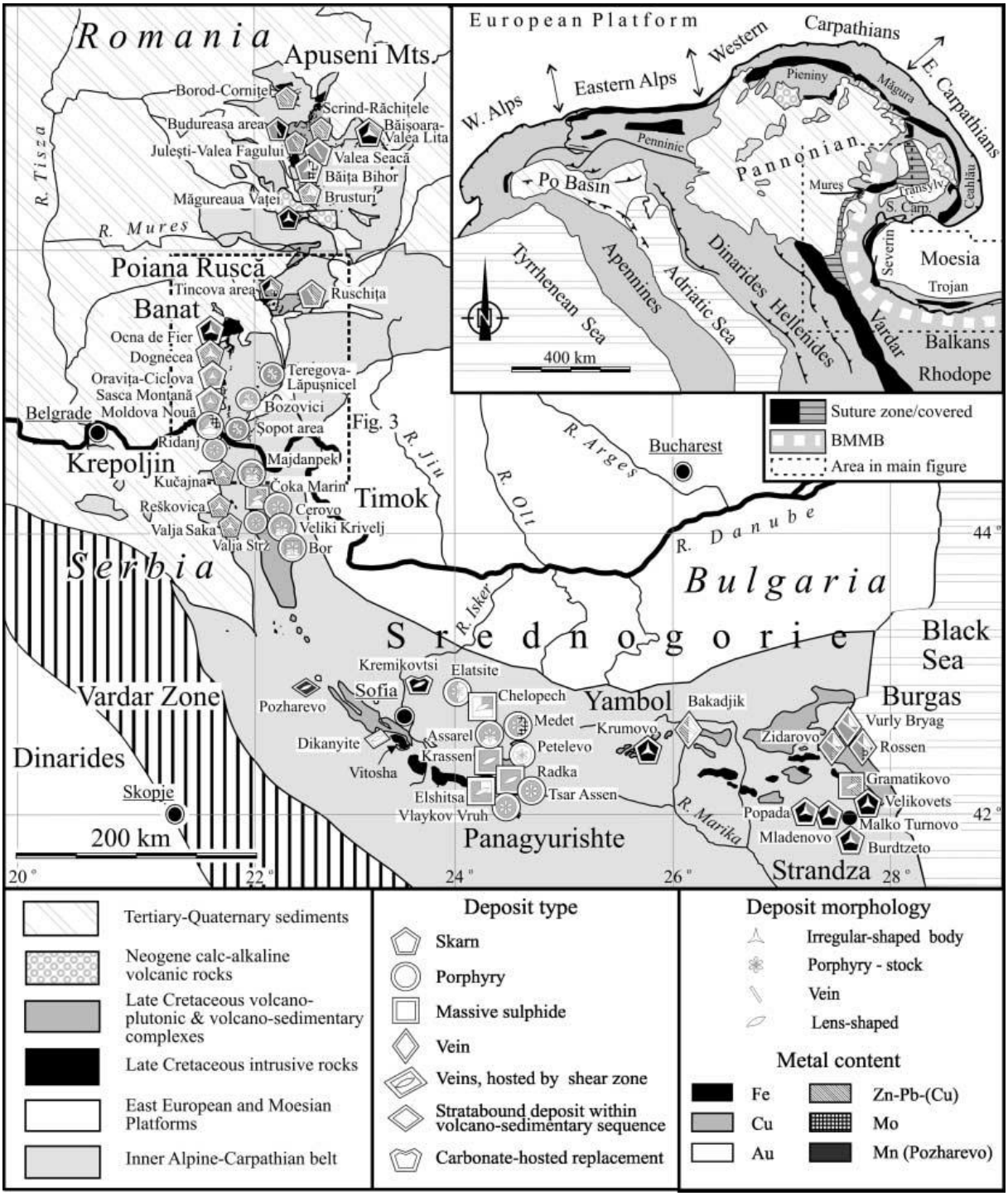

Fig. 3. Geological map showing the major ore deposits and the principal ore districts of southern Europe. The small inset shows the Banatitic Magmatic and Metallogenetic Belt (BMMB) within the geodynamic and structural domains within the Alpine-Balkan-Carpathian-Dinaride orogenic system (Ciobanu et al., 2002).

The metallic ores, especially of the northern part of the BMMB, have been exploited since pre-Roman times. The southern parts have been subject to renewed economic interest, which was followed by mining operations at Majdanpek, a large porphyry Cu-Au deposit in the Timok region and Chelopech, a high-sulfidation volcanogenic Cu-Au-As deposit in the central Srednogorie area (Berza et al., 1998). Today the most important deposits are the "[…] Cu-Ag mines at Moldova Nouă in Romania, Majdanpek, Veliki Krivelj and Bor in the Bor ore district in Serbia and Elatsite, Assarel and Chelopech of the Panagyurishte district in Bulgaria" (Ciobanu et al., 2002).

1.4. Gornja Lipa

The Gornja Lipa high-sulfidation epithermal porphyric deposit is situated in East Serbia (Fig. 4) in the Bor ore district, about 16 km NW of the town of Bor. The Bor ore district is characterized by an abundance of porphyry copper and associated high-sulfidation epithermal deposits. The metallogeny of the Bor ore district is comparable to the Panagyurishte ore district in Bulgaria and is part of the Timok Magmatic Complex (TMC), which is as well as the Panagyurishte ore district part of the Apuseni-Banat-Timok-Srednogorie belt (Heinrich and Neubauer, 2002; Ciobanu et

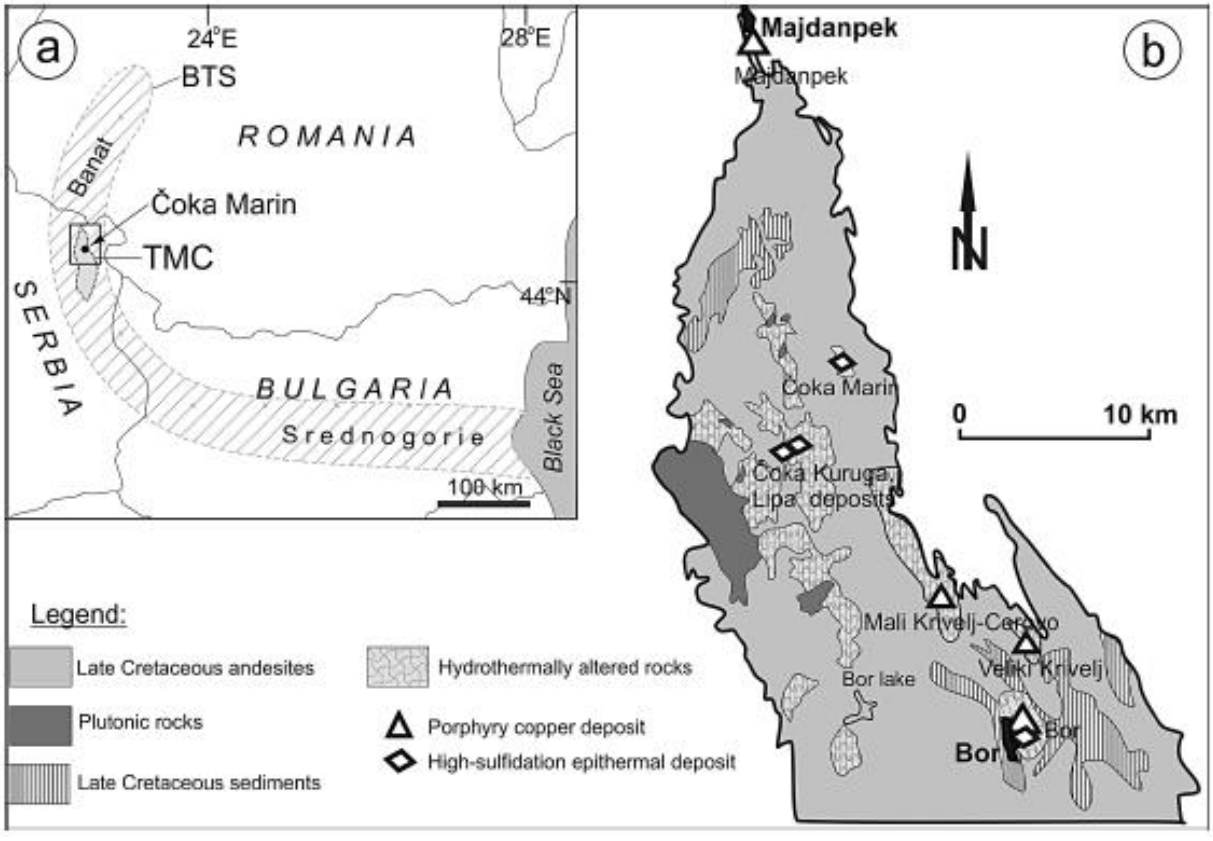

Fig. 4. (a) Location of the Timok Magmatic Complex (TMC) in the Apuseni-Banat-Timok-Srednogorie belt. (b) Geological map of the northern part of the Bor ore district (Pačevski et al. 2012.).

al., 2002). A detailed characterization of the Gornja Lipa deposit has been published by Drovenik (1958). It is discussed briefly by Rakić et al. (1978) and Jelenković et al. (2007). Radosavljević (1972) wrote an extensive diploma thesis about the mineral paragenesis of the Gornja Lipa deposit.

First geological explorations started after the end of the Second World War. The deposit was then mined over the next decades until most of the deposit was exploited in the year 1967, when mining operations were suspended. The mined ore was not directly processed on site, but transported to Bor for further enrichment. When the mine was closed about 500,000 t of unworked ore remained in mining area. The ore dumps left at the walls and floor of the deposit result in a continuous release of mine waters with low pH values (1.95) and elevated As and Fe contents (Dragisic et al., 1999, Dragišić et al., 2012). According to Jelenković et al. (2007) the ore reserves of the Gornja Lipa deposit are estimated at 1 Mt ore averaging 1.1% Cu, 13.26% S, 0.43% As, 3 – 6 g/t Au and 20 g/t Ag.

The Gornja Lipa deposit comprises one main stockwork ore body, hosted by strongly hydrothermally altered hornblende-augite andesite and volcanic breccia in a highly tectonized environment. The ore body is 150 m long, 80 m wide and was mined by open-pit method up to a depth of 100 m. The ore body is limited toward the east by a tectonic border, while in other directions the ore mineralization successively fades into the adjoining rocks.

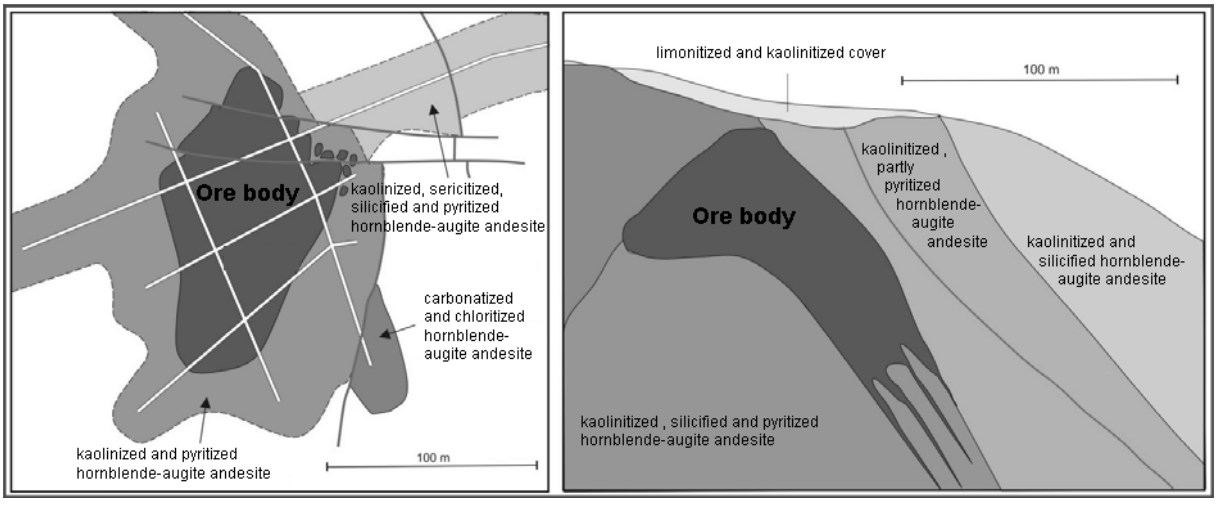

Fig. 5. Geological layout and cross-section of the Lipa ore deposit (modified after Jelenković et al., 2007)

The paragenesis of the ore body, as described by Drovenik (1958), Rakić et al. (1978), and Radosavljević (1972), is mainly comprised of pyrite and enargite, with minor to negligible amounts of luzonite, sphalerite, galena, covellite, chalcopyrite, stibioluzonite, chalcocite, melnikovite, chalcostibite, marcasite, stannite, magnetite, molybdenite, and neodigenite (Table 6). The ore body is irregularly pyritized, silicified, kaolinized, and alunitized. The surrounding rocks, hornblende-augite andesites, are for the most part strongly hydrothermally altered with different zones being distinguishable. Farthest from the ore body the hornblende-augite andesite is chloritized and carbonatized. The zones closer to the ore body are first pyritized and silicified and still closer pyritized and kaolinized. The different zones are especially differentiated in the eastern side of the deposit (Fig. 5).

1.5. Objectives

The objective of this Master thesis is a thorough characterization of the mineralogical composition of the waste material of the Gornja Lipa deposit. A mixture of different approaches and techniques offers the best possible overview of this rather complex mineral paragenesis. The pictorial documentation via reflected light microscopy and scanning electron microscopy was the starting point for the interpretation of the different ores, gangue minerals and weathering mineralizations. Additional phase analysis using X-ray powder diffractometry enabled an in-depth understanding of the mineral associations. The use of Raman spectroscopy and X-ray fluorescence spectroscopy allowed further mineralogical characterization. The objectives are:

a) the characterization and the distinction of both primary and secondary minerals;

b) the determination of the As-bearing minerals;

c) the evaluation of the alteration of the waste rock piles;

d) the pictorial documentation of the rock samples;

e) the application of various, complementary analytical techniques;

The analysis of waste rock material has been a frequently discussed topic over the last decades in earth sciences. The main focus, however, lays on the geochemical and environmental point of view with an emphasis on mine drainage waters and their

environmental impact. In comparison only few scientific studies focusing on the mineralogical characterization of mine wastes exist.

The Bor region in general is the subject of various scientific studies in rather diverse research fields (Antonijević and Mijatović, 2014; Ilić et al., 2011; Jankovic, 1990; Ranđelović et al., 2014; Šerbula et al., 2010; Stevanovich et al., 2011;).

There exist only two extensive mineralogical studies on the Gornja Lipa copper deposit; one publication by Drovenik (1958) and a diploma thesis by Radosavljević (1972). A short publication about the deposit was subsequently published by Rakić et al. (1978). Later on, only environmental and geochemical studies were conducted, focusing on arsenic contamination of the soil and water environment (Dragisic et al., 1999; Dangić and Dangić, 2007, Dragišić et al., 2012). In 2007 a field guide about ore deposits in the Carpathians, Balkans, Rhodope Massif and Caucasus was presented by Jelenković et al., containing a brief chapter about the Gornja Lipa deposit.

2. Samples

2.1. Sample Origin and Description

The samples (Fig. 8) used for the experimental work were collected in the summer of 2014 by Tamara Đorđević and Aleksandar Pačevski during a field trip visiting the abandoned copper deposit Gornja Lipa in the Bor Ore District, Serbia (Fig. 7). The intention of this field trip was the collection of different waste material samples from various points around the former mining area. Samples were collected in the abandoned mine pit as well as in the surrounding area composed of waste heaps and in the area of the bypassing Lipa river. Based upon macroscopic similarities the collected solid waste samples were divided into eleven groups. Furthermore soil samples and biofilms were collected. Those samples have yet to be analyzed and were not used in this thesis.

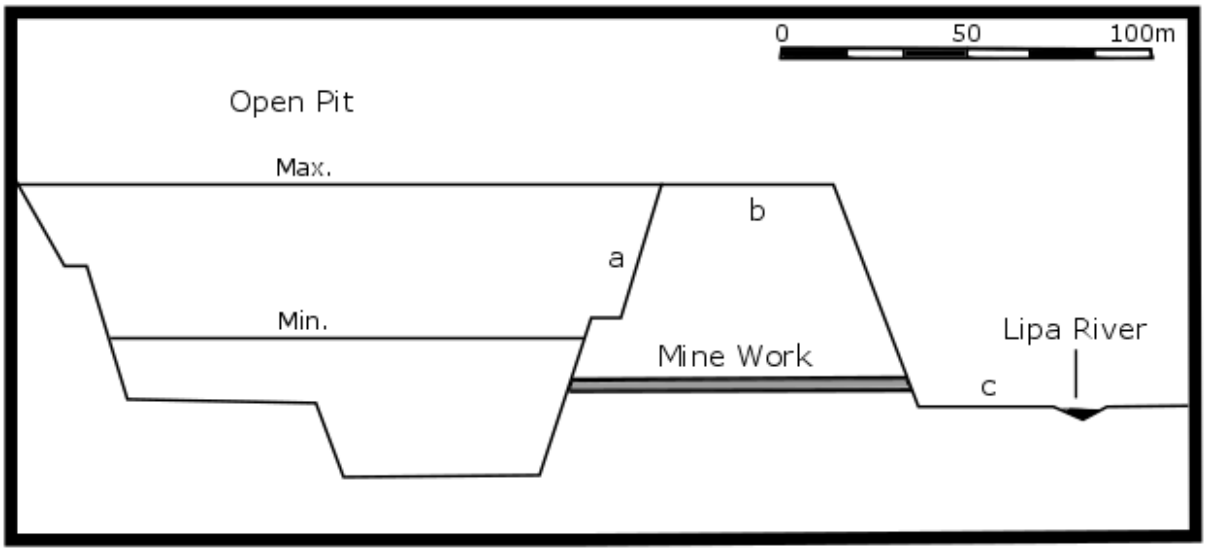

Fig. 6. Profile of the Gornja Lipa deposit. Sampling points (a, b, c) are shown. Samples 1-7 are from (c), samples 8 and 11 from (b), and samples 9-10 from (a) (modified after Dragisic et al., 1999).

Samples 1-7 were collected around point (c) of Fig. 6 and represent materials from oxidized waste heaps containing higher amounts of ores, macroscopically recognizable by a dark grey color and sometimes visible metallic luster of larger grains of ore. The samples consist of dense ore-rich aggregates (sample 2) to porous ore-poor to ore-rich samples (sample 1, 3-7). All of these samples 1-7 are covered by a white-greyish to yellow layer of secondary minerals. Sample 2 additionally has

areas with light brown to red alteration zones. Crystal size varies greatly between samples.

Sample 8 represents gangue material and is covered by a patchy fine layer of orange to dark red secondary minerals. The gangue material itself is homogenously light grey to very light brown. The sample was collected near point (b) of Fig. 6.

Sample 9 and 10 consist of severe oxidized material. The color is dark brown to red to orange and yellow. The samples are very brittle and easily break up. Sample 9 additionally shows a white, very soft layer, about 3 mm thick, on one side of the sample. Both samples were collected near point (a) of Fig. 6.

Sample 11 represents fibrous gypsum of white to light grey color collected near point (b) of Fig. 6. The gypsum aggregates are partially covered by ochre-colored secondary minerals.

2.2. Sample Preparation

The samples were prepared for analyses with different analytical methods. Polished thick sections of samples 1-7 and 9-10 were prepared for reflected light microscopy, Raman spectroscopic measurements and SEM-EDX analyses. For the SEM-EDX analyses the thick sections were polished and then coated with a thin layer of carbon to prevent the accumulation of electrostatic charge on the surface. Powdered samples were produced for X-ray powder diffractometry. The samples were crushed manually with the help of a small chisel and hammer, and thereafter finely ground with an agate mortar. Pellets were prepared for the XRF measurements with a hydraulic press. Additionally, selected crystals were removed from the surface of samples 3, 5, and 8-11 for single-crystal X-ray diffraction analyses.

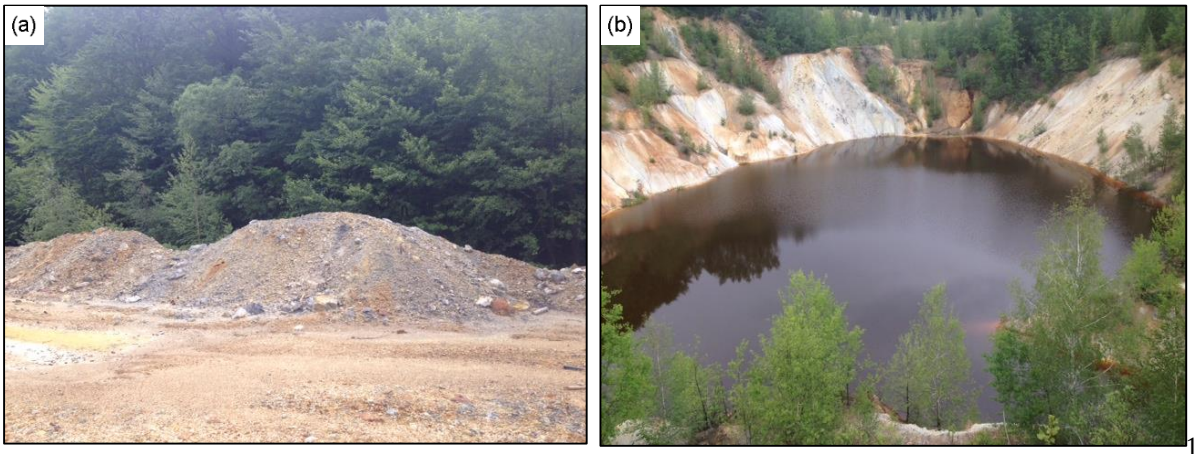

Fig. 7. Photographs of the sampling site at the Gornja Lipa deposit. (a) Mine waste heaps, (b) mine dump filled with meteoric water.

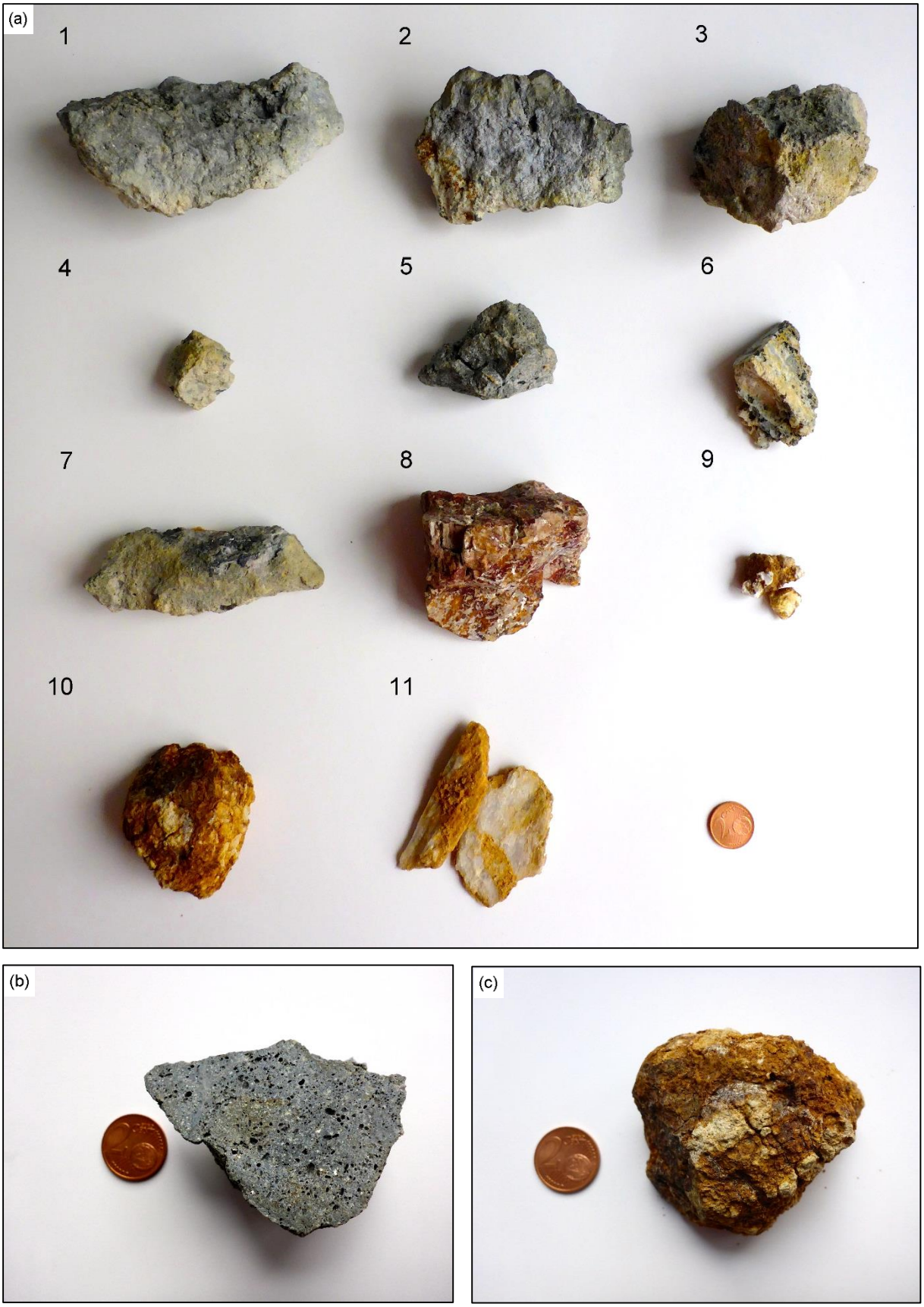

Fig. 8. Photographs of the solid mine waste mineral samples. (a) Overview of the 11 samples collected at the Gornja Lipa deposit site. Samples 1-7 are sulfide rich samples with grey to dark grey color. Sample 8-10 show heavily altered and oxidized samples. Sample 11 is fibrous gypsum covered with secondary iron minerals; (b) Close-up view of sample 5. Strongly altered rock with porous structure; (c) Close-up view of sample 10. Sample is coated by in secondary iron minerals.

3. Analytical Methods

3.1. Imaging techniques

The polished rock samples were first characterized by optical microscopy to obtain both detailed photographs and an overview of the ore associations and phase relationships as well as growth textures. A reflected-light microscope Olympus BX40 equipped with a 100 W halogen lamp and a bi-ocular with the objective lenses 5x/0.10, 20x/0.40, and 40x/0.75 was used. The samples were analyzed using plane-polarized light, as well as with cross-polarized light.

Overview pictures for the use as orientation guides in the consecutive scanning electron microscope analyses were taken with an Olympus BX51 microscope equipped with an Olympus DP70 digital camera system.

The scanning electron microscope (SEM) allows the detailed observation and characterization of mineralogical samples on a nanometer (nm) to micrometer (µm) scale. The SEM uses a finely focused electron beam which irradiates the sample. The electron beam can either be used to form an image through scanning over the sample surface or a specific point may be analyzed. Through the interaction of the electron beam with the sample secondary electrons, backscattered electrons, characteristic X-rays, etc. are produced. Secondary electrons and backscattered electrons are the primary signals used for high-resolution imaging. Through analyzing the characteristic X-rays emitted from the sample one can get elemental information as well as a qualitative to semiquantitative identification (Goldstein et al., 2003).

Secondary electron images and energy-dispersive X-ray spectroscopy of the polished rock samples were performed on a JEOL JSM-6610 LV instrument equipped with an energy-dispersive X-ray analysis (EDX) unit. The SEM-EDX system was used for semi-quantitative chemical analysis and recording high-resolution secondary-electron and backscattered-electron images. The samples were coated with a thin layer of carbon to prevent the accumulation of electric charge on the surface of the samples and thus avoid image artefacts. Electron images and EDX spectra were collected using an excitation voltage of 15 kV and spot size 49, at a working distance of 16 mm (optimum count rate for this SEM). The evaluation of the

X-ray spectra was carried out using the Bruker software Esprit (version 2.0) with PB-ZAF correction.

3.2. Powder X-ray diffraction

Powder X-ray diffraction is one of the most important tools to identify and quantify different phases in crystalline materials. It can also provide crystallographic information (unit-cell dimensions, crystal structure) and quantitative information about a sample.

Modern powder X-ray diffractometers consist of an X-ray generator, X-ray tube, sample holder and detector. There are two different configurations in use: The Bragg-Brentano theta-2theta and the Bragg-Brentano theta-theta setting. For the Bragg-Brentano theta-2theta geometry the sample is tilted in relation to the primary beam by an angle theta. Incident beam and reflected beam have the same angle in relation to the sample surface. The sample is rotated around the goniometer axis with the velocity ω, while the detector is moved with the velocity 2ω. The theta-theta configuration is based on a stationary sample, while the X-ray-tube and the detector are moving with a velocity ω around the sample. This horizontal setup not only allows the characterization of solid samples but also of liquids (Allmann, 2003; Spieß et al., 2005).

As the diffraction pattern for each phase is characteristic, one can use the position and relative intensity of a series of peaks and compare experimental data with reference patterns. Therefore, each phase characterization starts by comparison of the diffraction data with a comprehensive database of reference patterns (Powder Diffraction File, PDF, of the International Centre for Diffraction Data, ICDD).

A Phillips X'Pert powder X-ray diffractometer with Bragg-Brentano theta-2theta configuration, and scintillation counter with Cu*K*α radiation was used to get qualitative information about ten samples. The measured range was 5-75 °2θ for 3 s and a step size of 0.02 °2θ. The excitation voltage used was 40 kV and the electric current 40 mA. The powder samples were prepared using an agate mortar and pestle. 1-2 spatula tips of the powdered sample were then put on a Si sample holder and carefully flattened.

3.3. Single-crystal X-ray diffraction

Single-crystal X-ray diffraction is a method, which allows the identification of crystals by means of their lattice parameters. With the help of a crystal-structure refinement it also gives information about the three-dimensional spatial arrangement of atoms in a crystal structure.

Up to the 1970s, the measurements on diffractometers were conducted using film methods, since then mainly computer directed four-circle diffractometers are used, nowadays generally equipped with area detector systems. They dominate due to their higher accuracy and speed in comparison to film methods (Massa, 2011).

All four-circle diffractometer have three circles, which are used to rotate a crystal in relation to the incident X-ray beam. The fourth circle controls the position of the detector. In a measurement the crystal is oriented in relation to the incident X-ray beam to fulfil the Bragg condition and a reflection occurs. There are two main types of four-circle diffractometers:

- Eulerian geometry: The sample is mounted on the ω-circle, in the horizontal plane. Perpendicular to the primary beam is the vertical χ-circle, the goniometer head is movable along this circle but is mounted on a third axis, the φ-circle. The θ-circle is coaxial to the ω-circle and holds the detector.
- Kappa geometry: Here the setting of the ω-circle and θ-circle is identical to the eulerian geometry. But instead of a χ-circle there is a κ-circle, with an axis which is tilted by 50° in relation to the horizontal plane. Tilted by 50° to the κ-circle, the φ-circle is situated which holds the goniometer head.

Currently there are two types of area detectors used: the charge coupled device (CCD)-system, which is used to transform X-ray photons into electrical signals to be processed by a computer and the image plate, which is basically a re-writable memory foil (Massa, 2011).

For the identification of a crystal the lattice parameters, lattice type and crystal system will be determined. The acquired data sets will then be compared to different databases to validate if a known structure has been found.

A Nonius Kappa CCD single-crystal four-circle diffractometer was used. The diffractometer is equipped with a 300 µm diameter capillary-optics collimator and a

CCD area detector (621x576 pixels, binned mode); graphite-monochromatized Mo*K*α-radiation was used. The measurements were performed at room temperature (293 K). The technique was used to determine the types of crystals on the surface of the collected samples, further investigations like structure refinements were not scheduled.

3.4. X-ray fluorescence spectroscopy

X-ray fluorescence (XRF) spectroscopy is a widely used method relying on X-ray fluorescence for qualitative and quantitative material characterization. This technique is mainly used for bulk chemical analyses of major and trace elements.

Characteristic fluorescent X-rays are emitted by a sample excited by high-energy X-rays. The bombardment with high-energy X-rays leads to the striking out of an electron from the inner orbitals (lower energy levels, usually K and L shell) of an atom. The resulting hole causes the electronic structure of this atom to become unstable. The hole is then stepwise filled with electrons from outer orbitals (with a greater principal quantum number). This process causes energy to be released in the form of element-specific characteristic X-rays. The energy difference corresponds to the energy difference between the two involved orbitals.

There are two different measuring procedures available. Energy-dispersive spectrometry (EDXRF) uses a semiconductor detector to separate the emitted fluorescent radiation into its distinct energies whereas wavelength-dispersive spectrometry (WDXRF) uses a single crystal to diffract the fluorescent radiation into distinct angles.

An energy-dispersive XRF spectrometer Bruker Tracer IV SD with a 10 mm^2 X-flash silicon drift detector was used with excitation voltage of 40 kV. The samples were prepared using an agate mortar and pestle. The so prepared powder was then pressed into pellets using a hydraulic press. All XRD measurements were conducted in air.

3.5. Raman spectroscopy

Raman spectroscopy is a technique used for various applications, the most prominent among them being non-destructive phase characterization. Only small sample amounts in the range of a few cubic micrometers are needed. Another advantage is the possibility to analyze unprepared samples and to discriminate between polymorphs with the same chemical composition. For this thesis only polished samples were analyzed.

Raman spectroscopy is based on the Raman effect (Fig. 9, sketch 3) which describes an inelastic scattering process. More specifically it describes the change in wavelength when a laser beam interacts with the sample and in doing so with the molecular vibrational levels. There are two different types of inelastic scattering: Stokes and anti-Stokes type. The former describes the system gaining energy through the excitation of a phonon and the scattered photon losing the same energy amount whereas the latter originates from the excitation of an already vibrating system. The anti-Stokes scattering leads to the system releasing vibrational energy, which is then added to the energy of the light scattered. The bigger part of the radiation will be scattered elastically (Fig. 9, sketch 2), more precisely the molecule hit by a photon will keep its incident energy and the detected light will be of the same energy as the incident beam of light. This is called Rayleigh scattering. When the photon energy matches the energy difference between the two vibrational levels, infrared absorption may occur (Fig. 9, sketch 1).

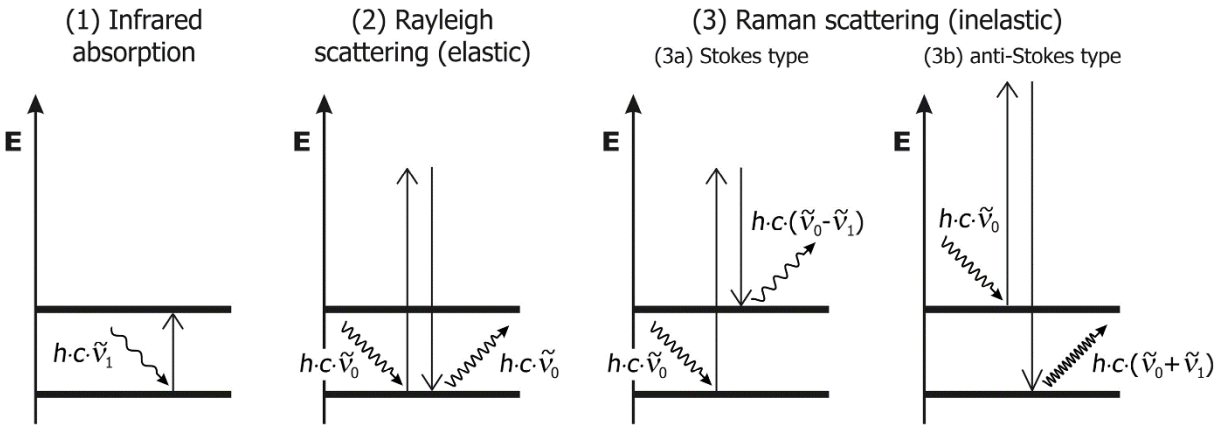

Fig. 9. Elucidation of the light-molecule interaction using a simplified energy level diagram. (1) Infrared absorption (2) Rayleigh scattering (3) Raman scattering with (3a) Stokes type and (3b) anti-Stokes type (Nasdala et al., 2004).

The obtained spectra are always plots of light intensity (usually in “a.u.”, arbitrary units) versus photon energy, the latter being transformed into wavenumbers (cm^{-1}). For practicality the use of absolute wavenumbers is not common, rather the Raman shift using the relative wavenumber is used (Nasdala et al., 2004).

A problem facing when analyzing sulfide minerals using Raman spectroscopy is the low number of available reference spectra as well as problems with the sulfide samples themselves. Sulfide minerals highly absorb laser light during measurements, there is often a poor peak/background ratio, and broad bands resulting from the fact that they are of weak Raman scattering power.

Measurements were carried out on a Horiba Jobin-Yvon LabRam HR Evolution Raman spectrometer and a Horiba Jobin-Yvon LabRam HR 800 Raman spectrometer, both equipped with an Olympus BX41 microscope and a CCD detector. All samples were excited using a 633 nm He-Ne-laser through a 50x long-distance objective lens. The holographic grating used was set to 1800 gr/mm and the confocal hole was opened to 1000 µm. To prevent damaging the highly absorbing sulfide-rich samples a filter had to be used. This prolonged the acquisition time up to 25 seconds using a 1% filter, which means that only 1% of the laser light reaches the sample surface. The acquisition time for non-sulfide minerals was 5 seconds. To obtain a fingerprint spectrum the range of 80 to 1200 cm^{-1} was measured.

The software PeakFIT® was used to calculate the band position; in the fit procedure combined Gaussian-Lorentzian band shapes were assumed after the background correction.

4. Results and Discussion

4.1. Imaging techniques

The use of reflected light microscopy is a most suitable technique for identifying opaque ore minerals. Pyrite (FeS_2), tennantite ($Cu_6[Cu_4(Fe,Zn)_2]As_4S_{13}$), enargite ($Cu_3AsS_4$), sphalerite (ZnS), galena (PbS) and chalcopyrite ($CuFeS_2$) were identified using typical characteristics such as color, reflectance, and grain shape (Fig. 10).

Pyrite, is easily identified by the characteristic yellowish white color as well as the high reflectance (R: 51.7%; Spry and Gedlinske, 1987) and hardness, exhibiting a high relief. It occurs with euhedral cubic and octahedral grain forms of sizes varying from 5 µm to 0.5 mm and anhedral crystalline masses. Most pyrites show, in addition to dissolution signs at the edges, holey, sponge-like areas usually in the inner parts of the grain (Fig. 10a), suggesting a zoning in the pyrite grains which indicates different deposition ages. Tennantite (R: 30-30.5%; Spry and Gedlinske, 1985) is recognizable with reflected-light microscopy by its medium grey color with a greenish tint. It occurs next to pyrite, sphalerite, and galena as small grains of about 20 µm in size. Internal reflections were not visible. Tennantite (Fig. 10a) grains are often intergrown with pyrite, filling holes and fissures indicating a later formation time. Additionally, tennantite is often a transformation product of enargite.

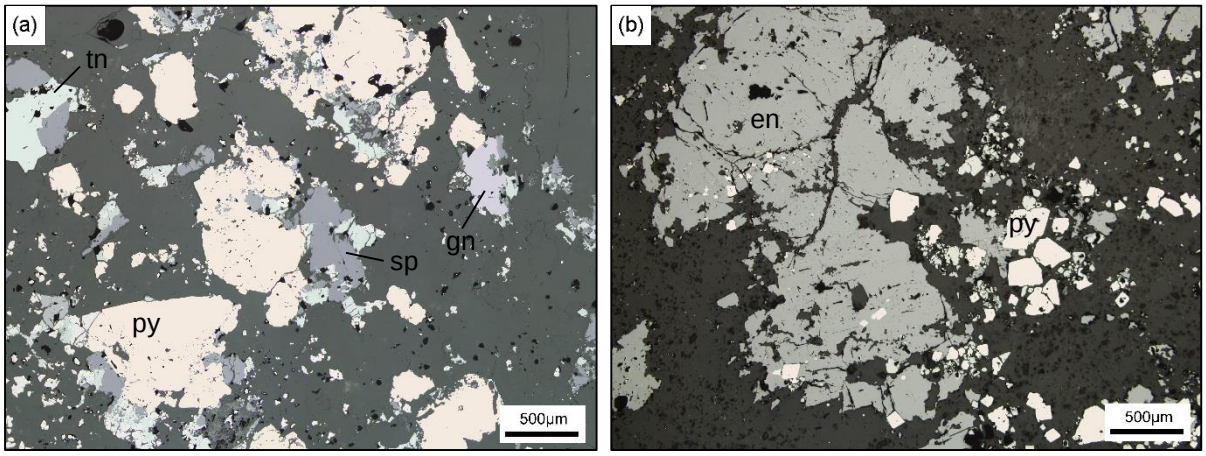

Fig. 10. Reflected light photomicrographs of selected mineral associations. (a) Overview of ore association in sample 6. Subhedral to euhedral grains of pyrite [py]; sphalerite [sp]; tennantite [tn] visible as a filler in holes and fissures of pyrite; also bigger grains of tennantite; galena [gn], with typical triangular pits. (b) Enargite [en] and euhedral pyrite [py].

Enargite (R: 24.2-25.2%; Spry and Gedlinske, 1985) is discernible by its light pinkish brown to pinkish grey color. It has a medium reflectance and a characteristic highly

colored anisotropy ranging from conspicuous violet, blue, green and red to orange. Enargite (Fig. 10b) is always intergrown with pyrite and has no distinctive grain shape. However some rectangular, tabular grains were observed. Grain sizes vary between a few µm to aggregates of about 2 mm. Sphalerite (R: 16.7%; Spry and Gedlinske, 1985) exhibits low reflectance and is therefore discernible by its relatively dark grey color in comparison to phases with higher reflectance. The grains mostly show strong signs of weathering. Sphalerite is often found next to tennantite filling fissures in pyrite. Galena (R: 43.1%; Spry and Gedlinske, 1985) is easily discernible by its high reflectance showing a white to light grey color. The perfect (100) cleavage leads to triangular pits (Fig. 10a), which are very characteristic for galena (Ramdohr, 1975). It is always associated with sphalerite and pyrite also showing signs of weathering. Chalcopyrite (R: 44.6-45%; Spry and Gedlinske, 1985) shows a strong reflectance with a characteristic yellow to brassy yellow color image.

Backscattered-electron (BSE) images allow an additional characterization of the gangue minerals, the matrix of the ore associations as well as the ore associations themselves. A distinction between primary and secondary phases is possible through close examination of the different samples. EDX analysis revealed a paragenesis typical for an argillic to advanced argillic alteration environment. The matrix comprises mainly quartz, kaolinite, diaspore, pyrophyllite and muscovite, with accessory rutile, barite, fluorapatite, titanite, chlorite and different aluminium phosphate-sulphate (APS) minerals.

Kaolinite (Fig. 11c) occurs mostly together with quartz, which features typically euhedral grains of varying sizes, often exhibiting hexagonal prism faces. Kaolinite shows large aggregates up to 200 µm evenly spread across the different samples with a pronounced flaky morphology. Diaspore is an infrequent constituent of the matrix; it is always intergrown with barite and quartz (Fig. 11b/d). Rectangular grain shapes occur as well as euhedral columnar grains up to 400 µm. Pyrophyllite appears as micaceous aggregates, as does muscovite. Pyrophyllite is a relatively common phase in the matrix. Muscovite is exhibiting sericitic characteristics, typical for a hydrothermal alteration environment; sericite being a common alteration product of orthoclase or plagioclase.

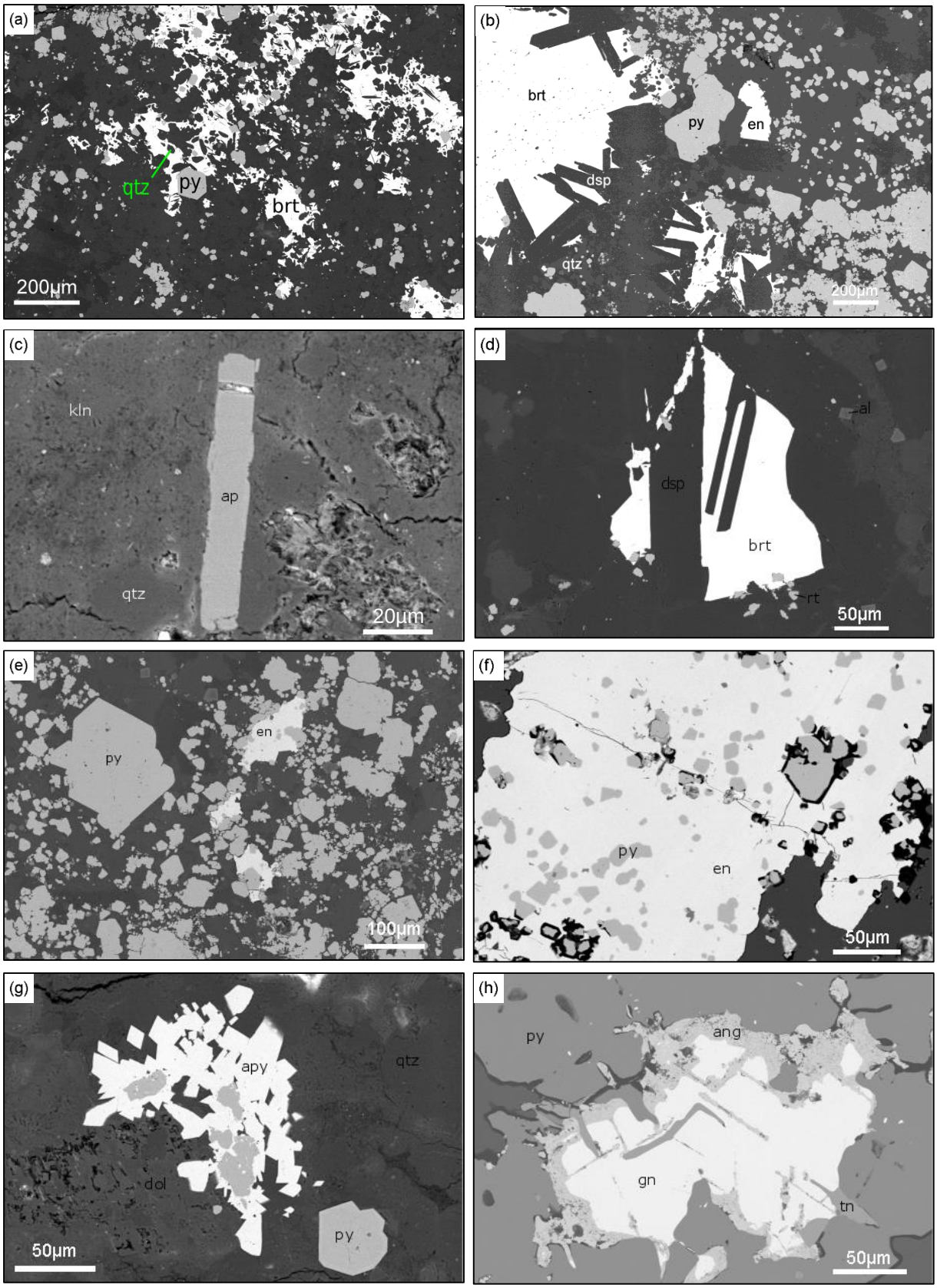

Fig. 11. Different backscattered-electron images. (a) and (b) Matrix Overview; quartz [qtz], pyrite [py], and barite [brt]. (c) Matrix close-up view of euhedral fluorapatite [ap] in quartz [qtz] and kaolinite [kln]. (d) Matrix close-up view of diaspore [dsp] growing in barite [brt], small rutile [rt] grains next to barite [brt]. (e) Main ore association; enargite [en] intergowing with pyrite [py]. (f) Pyrite [py] grains in enargite [en] matrix. Pyrite shows signs of dissolution connected with fissures in the enargite, leading to the

conclusion that enargite was formed after pyrite. (g) Euhedral to subhedral grains of arsenopyrite [apy] growing around pyrite [py] in a quartz [qtz] and zoned dolomite [dol] matrix. (h) Galena [gn] with an alteration rim of anglesite [ang] next to small grains of tennantite [tn] in a larger grain of pyrite [py].

Barite (Fig. 11a) is present as a relic and corroded phase, distributed unevenly among the different samples. It commonly contains small amounts of Sr. Also visible are inclusions of diaspore and quartz (Fig. 11b/d), which suggest a later formation time. Fluorapatite (Fig. 11c) shows distinctive signs of weathering along the edges instead of even prism faces. This indicates that the apatite survived the hydrothermal alteration and is of primary formation. It shows columnar to bulky shapes up to 80 µm in maximum dimension. The EDX analysis of different grains suggests a strongly F-dominant solid solution between the end-members of fluorapatite, hydroxylapatite, and chlorapatite. Additionally the analyzed apatites contain some minor impurities (e.g. Mg, Si, S, Fe) indicating an early, high-temperature formation.

No feldspars were found leading to the conclusion that they are already dissolved and transformed into new minerals during the hydrothermal alteration process.

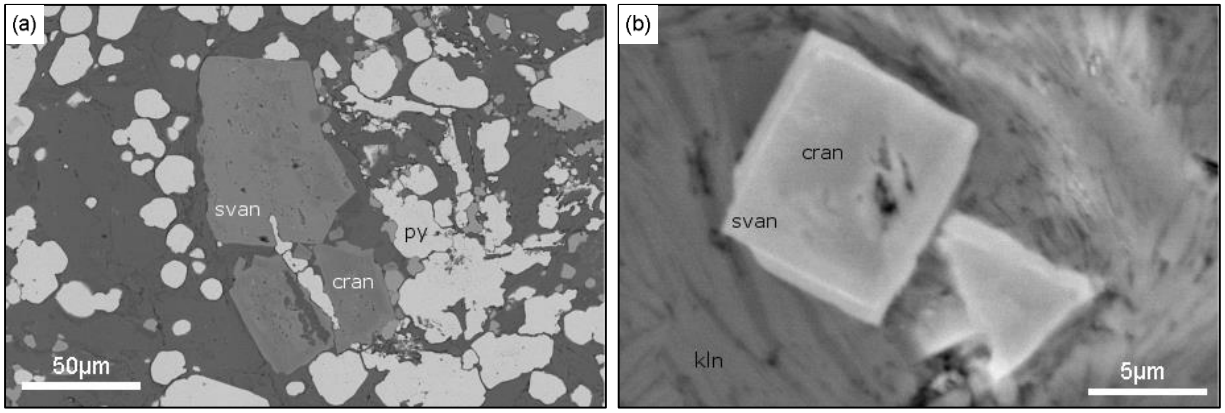

Fig. 12. Aluminium-phosphate-sulphate (APS) minerals. (a) Zoned minerals of svanbergite (svan) and crandallite next to pyrite py). (b) Zoned APS minerals with typical pseudocubic habit of svanbergite (svan) and crandallite (cran) next to kaolinite (kln).

The presence of several aluminium phosphate-sulphate (APS) minerals of the alunite supergroup was verified for the Gornja Lipa deposit. APS minerals are a large group of minerals, with more than 40 members, showing the general formula $DG_3(TX_4)_2X'_6$, where D is occupied by a large mono-, di-, or trivalent cation (K, Na, NH_4, Ca, Sr, Ba, Pb, REE) or partial vacancy, G is occupied by Al^{3+} or Fe^{3+}; T is S^{6+}, P^{5+} or As^{5+}; and X/X' is O, (OH), minor F and H_2O (Bayliss et al., 2010; Dill, 2001; Jambor, 1999). Pačevski et al. (2014) described the presence of svanbergite in the Gornja Lipa

deposit; the presence of crandallite, woodhouseite and svanbergite-goyazite was verified for the first time in the course of this thesis; svanbergite was also confirmed. Most grains form zoned, subhedral (Fig. 12a) to euhedral (Fig. 12b) grains of 5-100 µm in size. A thin, tabular to flaky morphology of the APS minerals is only observed rarely. The composition of APS minerals (Table 2) varies strongly among the analyzed mineral grains, and can be classified as crandallites (S-Sr-Ba-rich crandallite), woodhouseites (Sr-Ba-rich woodhouseite), svanbergites (close to endmember svanbergite, Ca-rich svanbergite, Ba-Ca-rich svanbergite) and svanbergite-goyazite (Ca-rich svanbergite-goyazite solid solution with goyazite-dominant composition). However, a general zonation pattern was observed: the central areas of the grains are often composed of crandallite and/or woodhouseite (i.e. Ca-dominant), whereas a more or less discernible rim consists of svanbergite and/or svanbergite-goyazite (i.e. Sr-dominant). Stoffregen and Alpers (1987) suggest that APS minerals form by "[…] replacement of apatite in the acidic, sulphate-rich environment that characterizes advanced argillic alteration". The Ba content is derived from the Ba content of the original feldspars, which is also the source of the Ba in barite. Trace impurity elements measured by EDS include Na, K, Fe, Ce, and F.

Table 2. Selected semiquantitative EDX data in at.% of svanbergite-goyazite (1-10), crandallite (11-13), svanbergite (14-34) and woodhouseite (35-36) from the Gornja Lipa deposit. Standardless data; several years of standardless analytical experience with this SEM-EDX combination and Bruker Esprit software give deviations below 5-10% from ideal values for common minerals. Estimated standard deviations for the present data are: for O ~2 at.%, F ~0.4 at.%, Na ~0.1 at.%, all other elements ~0.05 at.% (high contents) to ~0.1-0.2 at.% (low to trace contents).

Nr.	O	F	Na	Al	Si	P	S	K	Ca	Fe	Sr	Ba	Ce
1	68	1.1		15.01		7.40	2.79		3.06		2.61		0.11
2	68	1.7		14.79		7.46	2.63		2.55		2.85		
3	68	1.6		14.98	0.95	6.74	2.89		1.93		3.27		
4	67	1.6		14.74	1.11	7.12	2.58		1.55		3.33	0.23	0.29
5	69	1.8		14.18		7.23	3.02		1.50		3.65		
6	69	0.1		14.29	1.55	6.14	3.54		1.00		3.55		0.38
7	67	1.1		15.41		7.24	2.92		1.95	0.09	3.50	0.46	
8	68	1.2		14.77		7.51	2.61		2.78	0.22	2.73		
9	69	1.5		14.49		6.84	2.96		1.39		3.63		
10	69	0.7		14.71		7.24	2.76		2.93		2.65		
11	67	1.7	0.14	14.57		7.79	2.37		4.11		1.92	0.36	
12	67	1.4		15.33		7.49	2.41		3.60		2.06	0.20	
13	68	2.0		15.02		7.22	2.39		3.67		2.14		
14	69			14.81		5.33	5.11		0.72		4.56		
15	70			14.69	1.03	5.69	4.00		1.08	0.25	3.59		
16	69	1.2		14.37		5.73	4.24		1.01		3.99		
17	69	0.4		14.46		5.51	5.22		0.64		4.84		
18	69			15.33		5.53	4.82		0.44		4.89		
19	69		0.17	15.53		5.45	5.05	0.19	0.63		4.36		
20	69			15.03		5.44	5.19	0.07	0.71		4.44		
21	69			15.22		5.46	5.36		1.45		3.75	0.08	
22	66			16.88		6.11	5.26		0.93	0.23	4.73		
23	71			14.19		4.80	4.77		1.55		4.05		
24	70		0.37	13.83		4.97	5.48		0.58		3.83	0.52	
25	70		0.29	14.45		5.00	5.62		0.82		4.19		
26	72		0.21	13.12		4.82	4.92		0.41		3.38	0.93	
27	71		0.37	13.81		4.97	5.27		0.53		3.60	0.86	
28	69		0.37	14.09	1.63	4.82	5.19		0.90		3.09	0.48	
29	69		0.32	14.97	1.79	4.26	5.18	0.12	0.56		3.81		
30	69		0.37	15.51		4.62	5.33	0.16	0.56		4.26		
31	69		0.33	15.18		4.47	6.08	0.16	0.74		3.96		
32	69		0.55	14.87		4.38	6.16	0.31	0.71		3.70	0.12	
33	70			14.76		5.67	4.72	0.12	1.95		3.00	0.18	
34	70		0.27	15.14		5.13	4.87	0.25	1.52		2.93	0.14	
35	70			14.53		6.50	3.81		4.00		1.26		
36	69	0.5		14.38		6.21	4.79		2.79		2.39	0.42	

Many pyrites show zoning (Fig. 13) only visible on BSE images. This zoning is due to differences in the chemical composition. The lighter grey areas correspond to more or less As-rich regions, containing up to ~3.2 at.% of As according to EDX analyses (Fig. 14). Due to the different oxidation states of As it can be incorporated into the pyrite crystal structure as a substituent of either Fe or S. The EDX analyses (Fig. 14) suggest that As mainly substitutes S; however, only quantitative electron microprobe analyses could provide a reliable confirmation of this substitution scheme. In some pyrites the zoning reflects a change in the crystal habit during growth (Fig. 13a). The inner part mirrors an octahedron, whereas the outer part exhibits a cube-type habitus. Since the As-enrichment is observed predominantly in rim areas, a late-stage enrichment of the hydrothermal solutions with As is apparent.

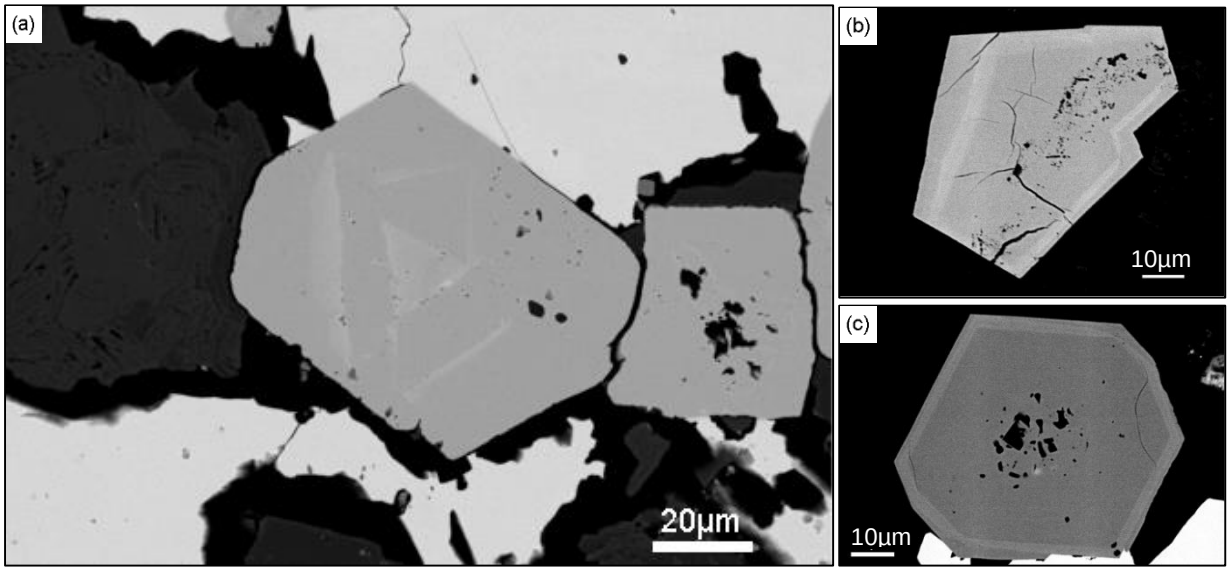

Fig. 13. (a), (b), and (c) backscattered-electron images of zoned pyrite. Most pyrite grains show a euhedral grain shape and a porous core. The brighter zones are As-rich domains.

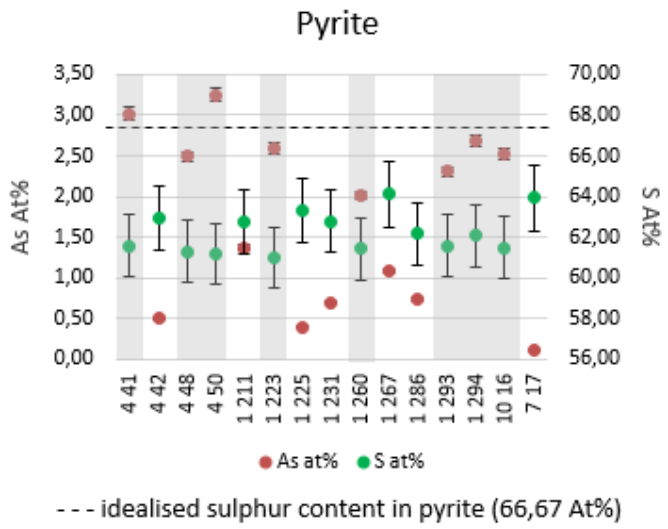

Fig. 14. EDX analysis results of arsenic (As) compared to sulfur (S) content in different pyrite samples. Showing also the idealized S content of 66.67 at.% in pyrite. Due to its ability to have different oxidation states As can be incorporated into the pyrite crystal structure instead of iron or sulphur. This graph suggests that As is mainly incorporated instead of S.

In sample 7 pyrite grains with a notable content of up to ~1.4 at.% Cu were found as inclusions in larger enargite grains (Fig. 11f), which suggests that enargite was formed at a later stage at increasing Cu^{2+} activities. This observation is also confirmed by the generally anhedral to irregular morphology of the enargite grains (Fig. 11e) intergrown with euhedral pyrite grains. Furthermore copper is a rather uncommon impurity in pyrite, which is due to crystallochemical differences between Cu^{2+} and Fe^{2+} ions. In the pyrite structure Fe is coordinated octahedrally by S. Due to the Jahn-Teller effect (Orgel, 1965) Cu^{2+} ions in the structure of pyrite are only stable in distorted octahedral sites, in regular tetrahedral sites or if a coupled Cu-X substitution occurs (Radcliffe and McSween, 1969). Therefore, only few localities with structurally bonded Cu in pyrite are known (Pačevski et al., 2008), one being the polymetallic Čoka Marin deposit, close to the Gornja Lipa deposit. Therefore, the detected Cu content is either structurally bonded or the result of submicroscopic inclusions of copper minerals. A clear determination would necessitate further investigation of this subject.

It was not possible to distinguish optically between enargite and luzonite (both ideally Cu_3AsS_4) with the help of the scanning electron microscope. While enargite and luzonite have the same chemical composition, enargite crystallizes in the orthorhombic crystal system and luzonite is tetragonal. One distinguishing feature is that enargite often forms quadratic to rectangular grains, while an anhedral grain

morphology, twinning and a high Sb content may indicate luzonite, which rarely forms well-formed crystals but generally rather fine-grained aggregates. The EDX analyses revealed Sb contents of up to 7 at.% Sb (Fig. 15); a high content of Sb nearly always correlates with a lower content of As, as Sb replaces As in the crystal structure. Pósfai and Buseck (1998) suggest that when enargite and luzonite are coexisting, luzonite generally contains a higher amount of Sb, i.e. the famatinite end-member component. The highest amount of Sb found in enargite is $Cu_3As_{0.8}Sb_{0.2}S_4$ (Gaines, 1957; Springer, 1969). A distinction thus can be made based on the Sb content found in the EDX analysis; 6 out of 30 spot analyses showed Sb contents too high for enargite and therefore are attributed to luzonite.

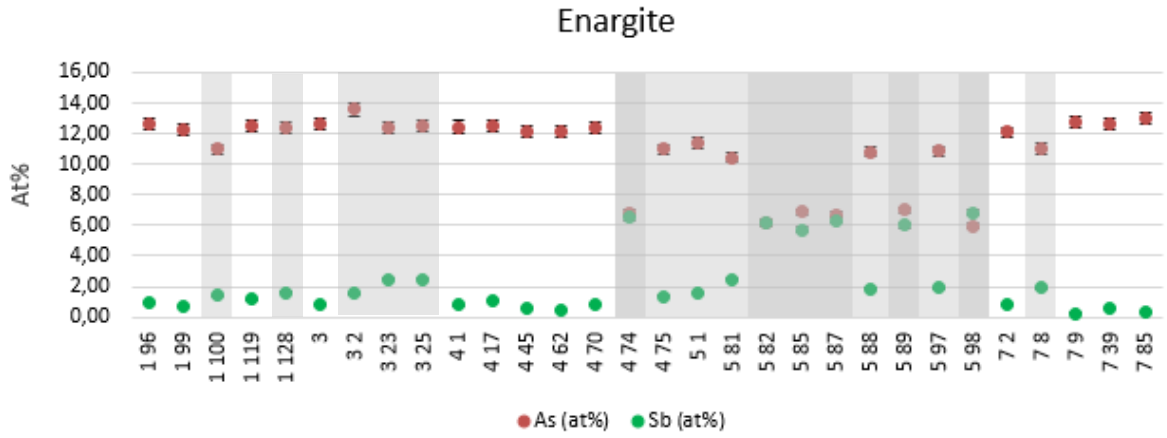

Fig. 15. EDX analysis of arsenic (As) and antimony (Sb) content in different enargite/luzonite samples. Marked in light grey are Sb-rich enargites, marked in dark grey are Sb-rich luzonites.

Besides the two main ore phases pyrite and enargite/luzonite, also other ore phases were characterized using EDX analysis. Arsenopyrite (Fig. 11g) forms well-shaped euhedral crystals, showing prismatic to rhomb-shaped cross-sections. Galena (Fig. 11h) exhibits a distinctive alteration rim of anglesite, a typical transformation product of galena in an acidic environment. The EDX analysis of Galena showed up to ~2.84 at.% Se. Tennantite (Fig. 11h) neighboring galena and anglesite is a common transformation product of enargite. Tennantite analyzed in sample 6 is Zn-rich and exhibits Zn values between ~6.44-7.49 at.% and Fe values between ~1.15-2.76 at.%. Accessory phases are chalcopyrite as an exsolution feature in pyrite, and tiny grains of colusite ($Cu_{12}VAs_3S_{16}$) and bornite, being typical minerals for a high-sulfidation epithermal-porphyry copper deposit. It is noteworthy that colusite is the only primary V-bearing sulfide observed during this study. A single tiny grain containing 28.39 at.% Au, 61.36 at.% Te and 12.25 at.% Cu was found in only one sample and could

not be identified due to the very small grain size; it may consist of two or more submicroscopic phases.

Stibnite was found in samples 5 and 7, and shows a typical perfect cleavage. It represents a late, relatively low-temperature formation. Small stibnite grains of 5-15 µm were found in sample 7 inside of larger enargite grains containing up to 4.5 at.% Cu. No publications were found supporting this high Cu content in stibnite, thus a mixture analysis is suggested based on the small grain size. In sample 5 one stibnite grain of 80 µm of size was found among other rather smaller grains, containing no Cu.

Limonite (Fig. 16) was only found in sample 10; the hand piece macroscopically consists of heavily oxidized material. The color is dark brown to red to orange and yellow, which already indicates the presence of limonite. In the BSE images limonite is visible at the edges of vugs and fissures, leading to the conclusion that it represents a secondary formation. Limonite exhibits desiccation cracks which indicates a crystallization from an original gel phase. The EDX analyses of limonite show a great number of impurities, for example up to ~0.2 at.% As.

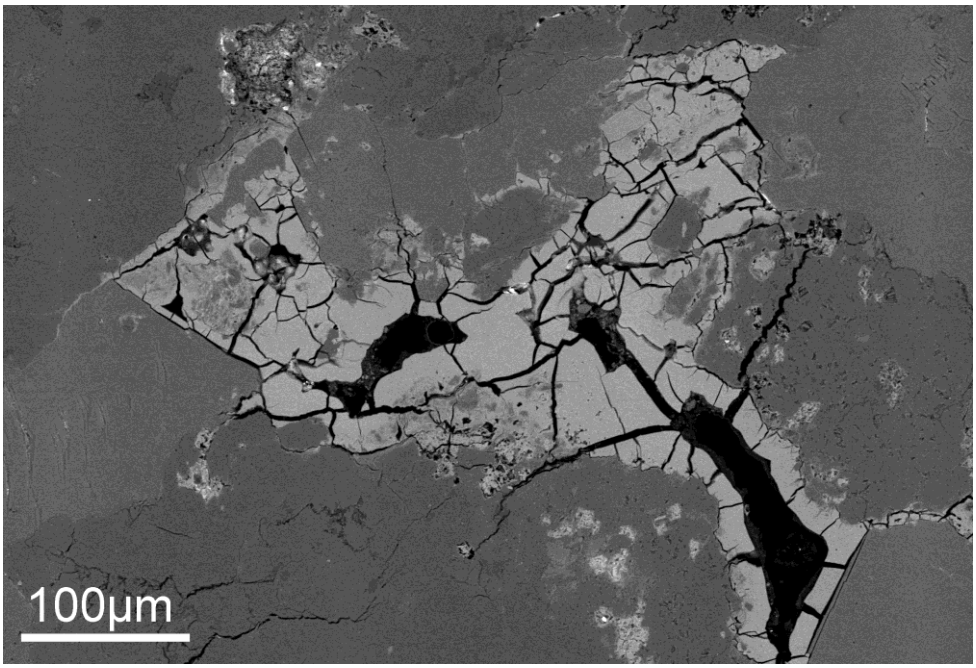

Fig. 16. BSE image of limonite (with desiccation cracks) visible at the edges of a vug in sample 10.

4.2. Powder X-ray diffraction

Powder X-ray diffraction allows the simultaneous characterization of different phases in a sample. An overview of the detected minerals is given in Table 3. Samples 1-7 (from oxidized waste heaps, containing higher amounts of ores) are comparable in their composition, containing sulfides as well as gangue minerals. Sample 1, 3, 4, 5, and 7 are similar, showing in the diffraction data peaks for pyrite as well as enargite and different amounts of the gangue minerals kaolinite, pyrophyllite, diaspore, barite, and quartz. The powder diffraction pattern of sample 2 is different, displaying only peaks for pyrite, muscovite, and quartz. Sample 6 is outstanding by its high content of sulfides, it contains, in addition to pyrite, also tennantite, sphalerite, and galena. The diffraction data of sample 8 (gangue material, covered by a fine layer of secondary minerals) is dominated by the gangue minerals quartz, kaolinite, and accessory rutile. Samples 9 and 10 (heavily oxidized material) show very different powder diffraction patterns. Sample 9 is macroscopically dominated by a white, very soft layer, about 3 mm thick on one side of the sample. The diffraction data shows mainly gypsum and small peaks of quartz, while other gangue minerals and sulfides are absent. In sample 10 enargite and tennantite are absent and quartz, gypsum, muscovite and dolomite are dominant. Also small peaks for pyrite were found in sample 10.

Table 3. Powder X-ray diffraction data of different samples of the Gornja Lipa deposit. Illustration of the phase distribution among the samples.

Mineral	Ideal formula	1	2	3	4	5	6	7	8	9	10
Pyrite	FeS_2	x	x	x	x	x	x	x			x
Tennantite	$Cu_6(Cu_4(Fe,Zn)_2)As_4S_{13}$						x				
Enargite	Cu_3AsS_4	x		x	x	x		x			
Sphalerite	ZnS						x				
Galena	PbS						x				
Kaolinite	$Al_2Si_2O_5(OH)_4$			x	x	x		x	x		x
Pyrophyllite	$Al_2Si_4O_{10}(OH)_2$	x			x						
Diaspore	AlO(OH)	x			x			x			
Barite	$BaSO_4$	x		x							
Rutile	TiO_2	x			x	x			x		x
Muscovite	$KAl_2(Si_3Al)O_{10}(OH)_2$		x	x							x
Anglesite	$Pb(SO_4)$						x				
Quartz	SiO_2	x	x	x	x	x	x	x	x	x	x
Gypsum	$Ca(SO_4)\ 2H_2O$									x	x
Dolomite	$CaMg(CO_3)_2$										x

4.3. Single-crystal X-ray diffraction

Single-crystal X-ray diffraction is a method using x-ray diffraction for the identification of crystals by means of their lattice parameters. The goal was the identification of crystals on the sample surface, ideally secondary formations formed through weathering of the primary material. The crystals scraped from the sample surface provided ambiguous results. Most crystal-like materials showed no clear results, being of X-ray amorphous nature. The diffraction pattern of some crystals showed diffraction rings, indicating a polycrystalline structure of the analyzed sample. Only few crystals provided definitive results. Samples 9_1, 10_2, 10_3 and 10_4, consisting of colorless acicular or thin tabular crystals, were identified as gypsum with the space group *C*2 and the cell parameters of *a*=6.28Å, *b*=15.24 Å, *c*=5.67 Å and *β*=113.91°. In sample 5, small clear, greenish crystals are visible in the porous structure of the rock. The X-ray single crystal diffraction of these extracted greenish crystals yielded elementary sulphur with the space group *F*222 and the cell parameters *a*=10.47 Å, *b*=12.87 Å and *c*=24.47 Å as a result.

Table 4. Single-crystal X-ray diffraction data of the samples of the Gornja Lipa deposit.

Sample	Crystal color	Result	Space group
3_1	greenish	amorphous	
3_2	yellowish	polycrystalline	
5_1	greenish	Sulphur	*F*222
5_2	greenish	Sulphur	*F*222
8_1	greenish	amorphous	
8_2	yellowish	amorphous	
8_3	yellowish	amorphous	
8_4	bluish	polycrystalline	
9_1	colorless	Gypsum	*C*2
9_2	colorless	amorphous	
10_1	reddish	amorphous	
10_2	colorless	Gypsum	*C*2
10_3	colorless	Gypsum	*C*2
10_4	colorless	Gypsum	*C*2
10_5	reddish	amorphous	

4.4. X-ray fluorescence spectroscopy

X-ray fluorescence spectroscopy is a technique most suitable for the qualitative and quantitative mineral characterization. It provides bulk chemical analyses of major and trace elements. This technique was used to get a qualitative overview of the basic

elementary composition of the samples. No quantitative measurements were attempted since they would necessitate the use of appropriate standards. See Table 5 for an overview of the results.

Sample 1 shows high intensities for Ba and Fe, medium intensities for S, Cu, and Sr, and low intensities for Al, Si, and As. These results correlate well with the EDX analyses and powder diffraction data for sample 1. The Fe and S content can be primarily assigned to the high amount of pyrite in the sample. The sulphur content can also be assigned to barite which also accounts for the high Ba peaks. Also enargite may account for part of the S peak as well as the observed Cu and As contents. The medium-high Sr peak may be explained by the presence of aluminium phosphate-sulphate (APS) minerals.

The X-ray fluorescence analysis of sample 2 gives rather different results with only two major peaks visible, corresponding to S and Fe. This fits especially well with the powder diffraction data, which only shows pyrite and minor contents of quartz and muscovite.

Sample 3 shows again different characteristics with high intensities for Fe, Cu, and As, medium intensities for Ba and low intensities for Si, S, and Sr. Compared to the EDX analysis and powder diffraction data these findings can easily be explained. The sample consists mainly of enargite, pyrite, and barite, which is in agreement with the high to medium high Fe, Cu, As, and Ba as well as minor S peaks. The Si and Sr peaks may be explained by the presence of quartz and barite (as well as APS minerals) respectively.

Sample 4 shows similar characteristics to sample 3, and exhibits high intensities for Cu and As, medium intensities for Fe, and low intensities for Si and S. A comparison with the EDX analytical and powder diffraction data explains the Cu, As, and S peaks with the presence of enargite, which is the main phase of this sample, along with quartz. Sample 5 demonstrates similarities to sample 2, but besides high intensities for S and Fe, it also exhibits medium intensity for Si and low intensities for Ti, Cu, As, and Sr. The S, Fe, Cu, and As contents can be explained by the presence of pyrite and enargite as determined bay the EDX analyses and powder diffraction data. The Ti and the Sr may be attributed to the occurrence of rutile and APS minerals. The EDX analysis indicates the presence of stibnite, yet no Sb could be detected.

Sample 6 exhibits altogether different results. It shows high intensities for Fe, Cu, Zn, As, and Pb, medium intensities for Si and S and low intensities for Sr. The presence

of these elements is explained by EDX analysis and powder diffraction data, and confirms the occurrence of pyrite, tennantite, sphalerite, galena and quartz.

Table 5. Qualitative X-ray fluorescence data of different samples of the Gornja Lipa deposit. Phase distribution marked as high content (+), medium content (o), and low content (-).

Mineral	Formula	1	2	3	4	5	6	7	8	9	10
Pyrite	FeS_2	+	+	o	-	+	+	+	-	-	+
Tennantite	$Cu_6(Cu_4(Fe,Zn)_2)As_4S_{13}$						+				
Enargite/luzonite	Cu_3AsS_4	o		+	+	-	+	+	o		-
Sphalerite	ZnS						+				o
Galena	PbS						+				
Chalcopyrite	$CuFeS_2$										-
Stibnite	Sb_2S_3							-			
Quartz	SiO_2	o		-	-	o	+	o	+		-
Rutile	TiO_2	-	-		-	-	-	-	+		-
Barite	$BaSO_4$	+		+							
Kaolinite	$Al_2Si_2O_5(OH)_4$	-		-	-			-			
Pyrophyllite	$Al_2Si_4O_{10}(OH)_2$	-		-	-			-			
Diaspore	AlO(OH)	-		-	-			-			
Gypsum	$Ca(SO_4)\cdot 2H_2O$									+	+
Limonite	FeO(OH)										+
Dolomite	$CaMg(CO_3)_2$										-
Calcite	$CaCO_3$										-

Sample 7 shows high intensities for Fe, Cu, and As, medium intensities for Si and S and low intensities for Sr and Sb. These findings correlate well with the EDX analysis and powder diffraction data for sample 7. The Fe and S content can be primarily assigned to pyrite and the Cu, As, and S content to enargite. The small Sr peak may be explained by the presence of APS minerals and the small Sb peak may be explained by the presence of stibnite and the minor Sb contents of enargite.

The X-ray fluorescence analysis of sample 8 gives completely different results with high intensities for Si and Fe, and medium intensities for Ti. The correlation to the powder diffraction data explains the Si and Ti peaks with the presence of quartz, which is the main phase of this sample, along with rutile.

Sample 9 exhibits besides the typical peaks for Fe and S, a high intensity peak for Ca. This can be explained by comparison to the powder diffraction data with the presence of gypsum. The high intensity of Fe may be explained by the presence of limonite including amorphous Fe oxide phases.

Sample 10 shows high intensities for Ca and Fe and medium to low intensities for Si, S, Ti, Cu, Zn, and As. The presence of these elements confirms the presence of pyrite, gypsum, rutile, and quartz detected by EDX analysis and powder diffraction data, and of sphalerite and limonite detected by EDX analysis.

Thus, the X-ray fluorescence analysis of the samples correlates very well with the analysis by energy-dispersive X-ray spectroscopy and X-ray powder diffraction and represents an essential confirmation of the previously obtained results.

4.5. Raman spectroscopy

Raman spectroscopy was used for the non-destructive phase characterization of polished thick sections. Fingerprint spectra were collected of all eight thick sections.

The results confirm the previous phase analyses, as all main ore and gangue phases could be detected (Table 5). Most importantly the presence of two previously unknown phases for the Gornja Lipa deposit could be verified. These phases are pyrophyllite, a common constituent of the matrix and svanbergite, an aluminium phosphate-sulphate member of the alunite supergroup.

Table 6. Raman spectroscopy data of different samples of the Gornja Lipa deposit. Illustration of the phase distribution among the samples.

Mineral	Ideal formula	1	2	3	4	5	6	7	10
Pyrite	FeS_2	x	x	x		x	x	x	x
Tennantite	$Cu_6(Cu_4(Fe,Zn)_2)As_4S_{13}$						x		
Enargite	Cu_3AsS_4			x	x		x	x	
Sphalerite	ZnS						x		
Galena	PbS						x		
Stibnite	Sb_2S_3							x	
Kaolinite	$Al_2Si_2O_5(OH)_4$							x	
Pyrophyllite	$Al_2Si_4O_{10}(OH)_2$	x			x				x
Diaspore	AlO(OH)	x			x				
Barite	$BaSO_4$			x					
Svanbergite	$SrAl_3(PO_4)(SO_4)(OH)_6$				x			x	
Rutile	TiO_2		x	x	x	x		x	x
Muscovite	$KAl_2(Si_3Al)O_{10}(OH)_2$			x					x
Quartz	SiO_2	x	x		x	x	x	x	x
Gypsum	$Ca(SO_4)\ 2H_2O$								x
Dolomite	$CaMg(CO_3)_2$								x

The svanbergite spectrum is dominated by an intense band at 1024 cm^{-1} (Fig. 17a). Some minor bands were detected at 176, 237, 365, 397, 481, 627, 998, 1003 and 1098 cm^{-1}. These band positions are in good agreement with Raman data published by Frost and Palmer (2011) about the molecular structure of svanbergite and also data in the RRUF internet database (Fig. 17a).

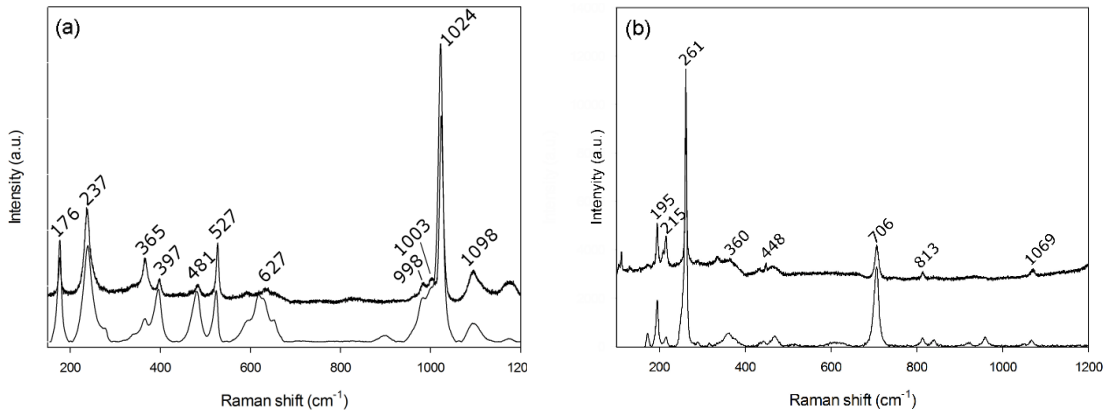

Fig. 17. Raman spectra of (a) svanbergite and (b) pyrophyllite with reference spectra (bottom spectra) from the RRUFF^{TM} database (www.rruff.info; pyrophyllite: R050051; svanbergite: R050549).

According to Wang et al. (2015) the first criterion to identify pyrophyllite is by the position of the strongest Raman peak (Si-O_b-Si mode). Dioctahedral and trioctahedral phyllosilicates may easily be mistaken for one another, however it is possible to distinguish between them as $v_{Si\text{-}Ob\text{-}Si} > 700$ cm^{-1} for dioctahedral and $v_{Si\text{-}Ob\text{-}Si} < 700$ cm^{-1} for trioctahedral groups. The Raman spectrum of Gornja Lipa pyrophyllite (Fig. 17b), being a dioctahedral phyllosilicate, shows a dominant peak at 706 cm^{-1}. Additional bands in range of the fundamental silicate vibrations are at 195, 215, 360, 448, 813, and 1069 cm^{-1}.

5. Conclusion

The intent of this master thesis is a thorough characterization of the solid waste material of the abandoned Gornja Lipa deposit in East Serbia. A mixture of different approaches and analytical techniques provided a broad spectrum of results for a rather complex mineral paragenesis.

The Gornja Lipa high-sulfidation epithermal-porphyry copper deposit belongs to the Bor metallogenic zone. The deposit, where active mining operations were ongoing until the mid-1960s, is a massive to disseminated mineralization in hydrothermally altered volcanic rocks. The ore body, which was pyritized, silicified, kaolinized, and alunitized, consists mainly of pyrite, enargite and luzonite, and subordinate to trace arsenopyrite, bornite, chalcopyrite, stibnite, colusite, galena, sphalerite, and tennantite. The accompanying minerals comprise quartz, muscovite, kaolinite, diaspore and pyrophyllite, with accessory rutile, barite, fluorapatite, titanite, and aluminium phosphate-sulphate (APS) minerals. Newly confirmed minerals for the Gornja Lipa deposit are bornite, arsenopyrite, stibnite, pyrophyllite, fluorapatite and the APS minerals crandallite, svanbergite-goyazite and woodhouseite.

Judging from the mineralogy of the deposit, it was expected to find the secondary Fe-arsenate-hydrate scorodite, as it represents a typical weathering product of Fe- and As-bearing deposits, but no scorodite could be found. This could be explained by the small amount of samples analyzed. A continuing study with a larger amount of samples would probably detect the presence of scorodite. The As-minerals enargite, tennantite arseonpyrite and colusite were identified; as As-bearing minerals pyrite with up to ~3.2 at.% As, antimonite with up to ~2.5 at.% As and limonite with up to ~0.24 at.% As were observed. Table 6 presents an overview of all phases identified during the present work and those reported in earlier studies on the Gornja Lipa deposit.

The occurrence of aluminium phosphate-sulphate (APS) minerals along with abundant kaolinite, diaspore, and pyrophyllite indicate conditions of argillic to advanced argillic alteration. These alteration environments can be linked to high-sulfidation epithermal copper mineralizations, which often occur in lithocaps above porphyry copper deposits. The type of high-sulfidation epithermal deposit offers a good description of the mineral paragenesis found at the Gornja Lipa deposit. The

deposit's mineralogy is similar to that of other transitional epithermal porphyry copper systems (e.g., *Kassiteres-Sapes*; Voudouris, 2014; several deposits discussed in Stoffregen and Alpers, 1987, Bajnóczi et al., 2004, and Georgieva and Velinova, 2012). Although alunite was not observed in the present study, its presence in the Gornja Lipa deposit is probable.

Table 7. List of all detected mineral phases with respective techniques used for identification, along with literature results of mineral phases reported in previous studies of the Gornja Lipa deposit. Given in italics are names of mineral groups, varieties, and non-IMA approved minerals, as well as obsolete names

Mineral	Ideal formula	SEM	pXRD	Raman	RLM	Drovenik (1958)	Jelenković et al. (2007)	Radosavljević (1972)	Rakić et al. (1978)
Pyrite	FeS_2	x	x	x	x	x	x	x	x
Tennantite	$Cu_6(Cu_4(Fe,Zn)_2)As_4S_{13}$	x	x	x	x			x	x
Enargite/luzonite	Cu_3AsS_4	x	x	x	x	x	x	x	x
Famatinite (*Stibioluzonite*)	Cu_3SbS_4					x		x	
Galena	PbS	x	x	x	x		x	x	
Bornite*	Cu_5FeS_4	x							
Covellite	CuS	x						x	x
Arsenopyrite*	FeAsS	x							
Chalcopyrite	$CuFeS_2$	x			x	x	x	x	x
Stibnite*	Sb_2S_3	x		x					
Colusite	$Cu_{12}VAs_3S_{16}$	x							x
Sphalerite	ZnS	x	x	x	x	x	x	x	
Chalcocite	Cu_2S					x		x	x
Melnikovite	amorphous, finely layered sulfide gel of pyrite/marcasite					x	x		x
Gold	Au						x	x(?)	x
Chalcostibite *(Wolfsbergite)*	$CuSbS_2$					x		x	x
Marcasite	FeS_2							x	x
Stannite	Cu_2FeSnS_4							x	x
Molybdenite	MoS_2							x	
Neodigenite	Cu_9S_5							x	
Limonite	FeO(OH)	x					x	x	
Kaolinite	$Al_2Si_2O_5(OH)_4$	x	x	x		x	x		
Pyrophyllite*	$Al_2Si_4O_{10}(OH)_2$	x	x	x					
Diaspore	AlO(OH)	x	x	x		x	x		
Barite	$BaSO_4$	x	x	x		x	x	x	x
Crandallite*[1)]	$CaAl_3(PO_4)(PO_3OH)OH)_6$	x							
Goyazite*[1)]	$SrAl_3(PO_4)(PO_3OH)OH)_6$	x							
Svanbergite[1)2)]	$SrAl_3(SO_4)(PO_4)OH)_6$	x		x					
Woodhouseite*[1)]	$CaAl_3(SO_4)(PO_4)OH)_6$	x							
Alunite	$KAl_3(SO_4)_2(OH)_6$	x				x		x	x
Cerussite	$PbCO_3$	x							
Rutile	TiO_2	x	x	x				x	
Muscovite ("*Sericite*")	$KAl_2(Si_3Al)O_{10}(OH)_2$	x	x	x		x			
Anglesite	$Pb(SO_4)$	x	x						
Quartz	SiO_2	x	x	x		x	x	x	x
Gypsum	$Ca(SO_4)\cdot 2H_2O$	x	x	x		x		x	
Dolomite	$CaMg(CO_3)_2$	x	x	x					x
Calcite	$CaCO_3$	x				x			x
Fluorapatite*	$Ca_5(PO_4)_3F$	x							
Titanite	$CaTiSiO_5$	x						x	
Chlorite (Chamosite)	$(Fe^{2+},Mg,Al,Fe^{3+})_5(Si,Al)_4O_{10}(O,OH)_8$	x				x	x		
Augite	$(Ca,Mg,Fe)_2Si_2O_6$					x			
Magnetite	Fe_3O_4					x		x	
Mn-Fe carbonate								x	
Leucoxene	mixture of Fe-Ti oxides							x	

SEM = energy-dispersive X-ray analysis in scanning electron microscope; pXRD = powder X-ray diffraction; Raman = Raman spectroscopy; RLM = reflected-light optical microscopy.
* Presence verified for the first time for the Gornja Lipa deposit.
1) APS minerals of the alunite supergroup
2) Svanbergite was also identified by Pačevski et al. (2014)

6. References

Allmann, R. (2003): Röntgenpulverdiffraktometrie: rechnergestützte Auswertung, Phasenanalyse und Strukturbestimmung. Springer: Berlin.

Antonijević, I. and Mijatović, P. (2014): The copper deposits of Bor, eastern Serbia: Geology and origin of the deposits. Geološki Anali Balkanskog Poluostrva, 75, 59-74.

Arribas, A. (1995): Characteristics of high-sulfidation epithermal deposits, and their relation to magmatic fluid. Mineralogical Association of Canada Short Course, 23, 419-454.

Bajnóczi, B., Seres-Hartai, É., Molnár, F., and Nagy, G. (2004): Phosphate-bearing minerals in advanced argillic alteration zones of high-sulphidation ore deposits in the Carpatho-Pannonian region. Acta Mineralogica-Petrographica, 45, 85-92.

Bayliss, P., Kolitsch, U., Nickel, E.H., and Pring, A. (2010): Alunite supergroup: recommended nomenclature. Mineralogical Magazine, 74(5), 919-927.

Berza, T., Constantinescu, E. and Vlad, S. N. (1998): Upper Cretaceous magmatic series and associated mineralisation in the Carpathian-Balkan Orogen. Resource Geology 48(4), 291-306.

Ciobanu, C.L., Cook, N.J., and Stein, H. (2002): Regional setting and geochronology of the Late Cretacious Banatitic Magmatic and Metallogenetic Belt. Mineralium Deposita 37(6-7), 541-567.

Dangić, A., and Dangić, J. (2007): Arsenic in the soil environment of central Balkan Peninsula, southeastern Europe: occurrence, geochemistry, and impacts. Trace Metals and other Contaminants in the Environment, 9, 207-236.

Dill, G. (2001): The geology of aluminium phosphates and sulphates of the alunite group minerals: a review. Earth Science Reviews, 53(1), 35-93.

Dragisic, V., Vrvic, M., Milenic, D., and Miladinovic, B. (1999): Mine Waters and Waters of Copper Deposit Tailing Disposals of Serbia and Environmental Protection. Hydrogeochemical aspect. International Mine Water Association International Congress: Mine/Quarry: Waste Disposal & Closure – Mine Water & Environment for the 21st Century, Sevilla, Spain, 527-533.

Dragišić, V., Atanacković, N., Živanović, V., and Milentijević, G. (2012): Physicochemical characteristics of mine waters at abandoned mining sites in Serbia. Geologica Macedonica, 3, 355-360.

Drovenik, M. (1958): Bakrovo Rudišče Gornja Lipa. Geologija, 4, 63-78 (in Slovenian with English abstract).

Einaudi, M.T., Hedenquist, J.W., and Inan, E.E. (2003): Sulfidation State of Fluids in Active and Extinct Hydrothermal Systems: Transitions from Porphyry to Epithermal Environments. Society of Economic Geologists, Special Publication, 10, 285-314.

Frost, R.L. and Palmer, S.J. (2011): Molecular structure of the mineral svanbergite SrAl3(PO4,SO4)2(OH)6 – A vibrational spectroscopic study. Journal of Molecular Structure, 994(1), 232-237.

Gaines, R.V. (1957): Luzonite, famatinite, and some related minerals. American Mineralogist, 42, 766-779.

Goldstein, J.I., Newbury, D.E., Echlin, P., Joy, D.C., Lyman, C.E., Lifshin, E., Sawyer, L., and Michael, J.R. (2003): Scanning electron microscopy and X-ray microanalysis. Kluwer Academic, Plenum Publ.: New York.

Georgieva, S. and Velinova, N. (2012): Alunite from the advanced argillic alterations in the Chelopech high-sulphidation epithermal Cu-Au deposit, Bulgaria: Chemistry, morphology and genetic significance. Geochemistry, Mineralogy and Petrology, 49, 17-31

Hedenquist, J.W., Arribas, A., Jr., and Gonzalez-Urien, E. (2000): Exploration for epithermal gold deposits. Reviews in Economic Geology, 13, 245-277.

Heinrich, H.A. and Neubauer, F. (2002): Cu-Au-Pb-Zn-Ag metallogeny of the Alpine-Balkan-Carpathian-Dinaride geodynamic province. Mineralium Deposita, 37(6), 533-540.

Hippolyte, J.C., Bădescu, D., and Constantin, P. (1999): Evolution of the transport direction of the Carpathian belt during its collision with the east European Platform. Tectonics, 18(6), 1120-1138.

Ilić, I., Bogdanović, D., Živković, D., Milošević, N., and Todorović, B. (2011): Optimization of heavy metals total emission, case study: Bor (Serbia). Atmospheric Research, 101(1), 450-459.

Jambor, J.L. (1999): Nomenclature of the Alunite Supergroup. The Canadian Mineralogist, 37, 1323-1341.

Jankovic, S. (1990): Types of copper deposits related to volcanic environment in the Bor district, Yugoslavia. Geologische Rundschau, 79(2), 467-478.

Jelenković, R., Banjesević, M., Cvetković, V. and Pačevski, A. (2007): Advances in Regional Geological and Metallogenic Studies in the Carpathians, Balkans, Rhodope Massif and Caucasus (Romania, Serbia, Bulgaria and Georgia) - A field conference, September 4-7, 2007, Rtanj Balasevic Motel, Bor area, Serbia, Field Guide, 42 pp.

Linzer, H.G., Frisch, W., Zweigel, P., Girbavea, R., Hann, H.P., and Moser, F. (1998): Kinematic evolution of the Romanian Carpathians. Tectonophysics, 297(1),133-156.

Massa, W. (2011): Kristallstrukturbestimmung. Vieweg + Teubner: Berlin.

Nasdala, L., Smith, D.C., Kaindl, R., and Ziemann, M.A. (2004): Raman spectroscopy: Analytical perspectives in mineralogical research. In: Beran, A. and Libowitzky, E., Eds., Spectroscopic methods in mineralogy, European Mineralogical Union Notes in Mineralogy, 6. Eötvös University press, Budapest, 281-343.

Neugebauer, J., Greiner, B., and Appel, E. (2001): Kinematics of the Alpine–West Carpathian orogen and palaeogeographic implications. Journal of the Geological Society, 158(1), 97-110.

Neukirchen, F. and Ries, G. (2014): Die Welt der Rohstoffe: Lagerstätten, Förderung und wirtschaftliche Aspekte. Springer Berlin Heidelberg: Berlin, Heidelberg.

Orgel, L.E. (1965): An introduction to transition-metal chemistry: ligand-field-theory. Taylor & Francis.

Pačevski, A., Libowitzky, E., Živković, P., Dimitrijević, R., and Cvetković, L. (2008): Copper-bearing pyrite from the Čoka Marin polymetallic deposit, Serbia: mineral inclusions or true solid-solution? The Canadian Mineralogist, 46(1), 249-261.

Pačevski, A., Moritz, R., Kouzmanov, K., Marquardt, K., Živković, P., and Cvetković, L. (2012): Texture and composition of Pb-bearing pyrite from the Čoka marin polymetallic deposit, Serbia, controlled by nanoscale inclusions. The Canadian Mineralogist, 50(1), 1-20.

Pačevski, A., Šarić, K., Cvetković, V., and Banješević, M. (2014): Aluminum phosphate-sulfate (APS) minerals in the Bor metallogenic zone, Serbia. Proceedings of the 16thSerbian Geological Congress, Donji Milanovac, Serbia, May 22-25, 281-284

Pósfai, M.L. and Buseck, P.R. (1998): Relationships between microstructure and composition in enargite and luzonite. American Mineralogist, 83, 373-382.

Radcliffe, D. and McSween, H.Y. (1969): Copper zoning in pyrite from Cerro de Pasco, Peru: a discussion. American Mineralogist, 54(7-8), 1216-1217.

Radosavljević, S. (1972): Mineral paragenesis of copper deposit Gornja Lipa. Diploma Thesis, Faculty of Mining and Geology, University of Belgrade, 75 pp. (in Serbian).

Rakić, S., Radosavljević, S., and Dimitrijević, R. (1978): A member of luzonite-famatinite (stibioluzonite) series from the ore deposit Gornja Lipa. Extrait des Comptes Rendus des Séances de la Société Serbe de Géologie, pour l'année 1977, 35-40 (in Serbian with english summary).

Ramdohr, P. (1956): Die Erzmineralien und ihre Verwachsungen. Akademie-Verlag: Berlin.

Ranđelović, D., Cvetković, V., Mihailović, N., and Jovanović, S. (2014): Relation between edaphic factors and vegetation development on copper mine wastes: A case study from Bor (Serbia, SE Europe). Environmental Management, 53(4), 800-812.

Rye, R.O., Bethke, P.M., and Wassermann, M.D. (1992): The stable isotope geochemistry of acid-sulfate alteration. Economic Geology, 87(2), 225-267.

Săndulescu, M. and Visarion, M. (2000): Crustal structure and evolution of the Carpathian–western Black Sea areas. First Break, 18(3), 103–108.

Sillitoe, R.H. (2010): Porphyry copper systems. Economic Geology, 105(1), 3-41.

Sillitoe, R.H. and Hedenquist, J.W. (2003): Linkages between volcanotectonic settings, ore-fluid compositions, and epithermal precious metal deposits. Society of Economic Geologists, Special Publication, 10, 315-343.

Šerbula, S.M., Antonijević, M.M., Milošević, N.M., Milić, S.M., and Ilić, A.A. (2010): Concentrations of particulate matter and arsenic in Bor (Serbia). Journal of Hazardous Materials, 181(1), 43-51.

Spieß, L., Schwarzer, R., Behnken, H., and Teichert, G. (2005): Moderne Röntgenbeugung: Röntgendiffraktometrie für Materialwissenschaftler,Physiker und Chemiker. Teubner: Wiesbaden.

Springer, G. (1969): Compositional variations in enargite and luzonite. Mineralium Deposita, 4(1), 72-74.

Spry, P.G. and Gedlinske, B.L. (1987): Tables for determinations of common opaque minerals. Economic Geology Publishing Company, New Haven.

Stevanovic, Z.O., Antonijevic, M.M., Bogdanovic, G.D., Trujic, V.K., and Bugarin, M.M. (2011): Influence of the chemical and mineralogical composition on the acidity of an abandoned copper mine in the Bor river valley (eastern Serbia). Chemistry and Ecology, 27(5), 401-414.

Steven, T.A. and Ratté, J.C. (1960): Geology and ore deposits of the Summitvilee district, San Juan Mountains, Colorado. U.-S.-Geological Survey. Prof. Paper 343.

Stoffregen, R.E. (1987): Genesis of acid-sulfate alteration and Au-Cu-Ag mineralization at Summitville, Colorado. Economic Geologist, 82, 1575-1591.

Stoffregen, R.E. and Alpers, C.N. (1987): Woodhouseite and svanbergite in hydrothermal ore deposits; products of apatite destruction during advanced argillic alteration. The Canadian Mineralogist, 25(2), 201-211.

Strashimirov, S. and Popov, P. (2000): Geology and metallogeny of the Panagyurishte region (Srednogorie zone, Bulgaria). IN Guide to Excursions Aand C, ABCD-GEODE Workshop, Borovets, Bulgaria, 50.

Voudouris, P.C. (2014): Hydrothermal corundum, topaz, diaspore and alunite supergroup minerals in the advanced argillic alteration lithocap of the Kassiteres-Sapes porphyry-epithermal system, western Thrace, Greece. Neues Jahrbuch für Mineralogie - Abhandlungen: Journal of Mineralogy and Geochemistry, 191(2), 117-136.

Wang, A., Freeman, J.J., and Jolliff, B.L. (2015): Understanding the Raman spectral features of phyllosilicates. Journal of Raman Spectroscopy, 46(10), 829-845.

White, N.C. and Hedenquist, J.W. (1995): Epithermal gold deposits: styles, characteristics and exploration. SEG Newsletter, 23(1), 9-13.

Zweigel, P., Ratschbacher, L. and Frisch, W. (1998): Kinematics of an arcuate fold-thrust belt: the southern Eastern Carpathians (Romania). Tectonophysics, 297(1), 177-207.

Appendix I – List of figures

Appendix II – List of tables

Appendix IV – Curriculum vitae

Personal Details

Name	Tamina Buttinger-Kreuzhuber
Date of Birth	12/08/1989
Nationality	Austrian
E-mail	mail@tamina.at

Education

Since 04/2014	Master of Science - Earth Sciences with focus on Mineralogy and Crystallography - University of Vienna Thesis advisors: Ao. Univ-Prof. Dr. Christian L. Lengauer and Dr. Tamara Đorđević
07/2013	Short course - University of Vienna “Luminescence Spectroscopy and Imaging in Geosciences" Pre-conference short course of CORALS-2013 (Conference on Raman and Luminescence Spectroscopy)
04/2010 - 03/2014	Bachelor of Science - Earth Sciences - University of Vienna Bachelor Thesis: „Optische und chemische Analyse einer Nickelerzparagenese der Zinkwand in den Schladminger Tauern” Thesis advisor: Ao. Univ-Prof. Dr. Eugen Libowitzky
09/2009 - 02/2010	Bachelor of Science - Geosciences - University of Bremen

Working experience

09/2015 - 12/2015	Research Assistant Geologische Bundesanstalt
11/2014 - 04/2015	Research assistant within the project „Structural Chemistry of Environmentally Relevant Arsenic Compounds“ (FWF, Graduate Scholarship) University of Vienna - Institute of Mineralogy and Crystallography
04/2014 - 12/2014	Research Assistant Geologische Bundesanstalt
03/2014 - 07/2014	Teaching assistant “Mineralogy 1 – Rock forming Minerals” University of Vienna - Institute of Mineralogy and Crystallography

10/2013 - 02/2014	Teaching assistant “Mineralogy 2 – Ore and Industrial Minerals”
	University of Vienna - Institute of Mineralogy & Crystallography
04/2013 - 03/2014	Buffet employee
	Mayer am Pfarrplatz
07/2012 - 08/2012	Research assistant
	University of Natural Resources and Life Sciences - Department of Crop Sciences
03/2014 - 07/2014	Teaching assistant “Mineralogy 1 – Rock forming Minerals”
	University of Vienna - Institute of Mineralogy and Crystallography
08/2008 - 08/2009	European Voluntary Service
	Øhavets Smakkecenter, Denmark

Language skills

German	Native language
English	Fluent
Danish	Good knowledge
Spanish	Basic knowledge
French	Basic knowledge

Publication

Buttinger-Kreuzhuber, T., Kolitsch, U., Pačevski, A., and Đorđević, T. (2015): Aluminium phosphate-sulphate (APS) minerals in the Gornja Lipa deposit, Bor district, Serbia. Poster, MinPet 2015, Leoben, Austria, September 10-13; abstract in Mitt. Österr. Mineral. Ges. 161, 30.